[redacted]

HIGH–STRENGTH FIBER–OPTIC WAVEGUIDE

A134931

G.D. Robertson

Hughes Research Laboratories

3011 Malibu Canyon Road

Malibu, CA 90265

November 1978

MDA–903–78–C–0289

Quarterly Report 1

For period 9 April through 31 July 1978

ARPA Order No. 3591

Approved for public release; distribution unlimited.

Sponsored by

DEFENSE ADVANCED RESEARCH PROJECT AGENCY (DoD)

1400 Wilson Boulevard

Arlington, VA 22209

The views and conclusions contained in this document are those of the author and should not be interpreted as necessarily representing the official policies, either express or implied, of the Defense Advanced, Research Projects Agency or the United States Government.

ARPA Order Number	3591
Name of Contractor	Hughes Research Laboratories
Effective Date of Contract	1 May 1978
Contract Expiration Date	9 April 1979
Contract Number	MDA 903-78-C-0289
Name and Phone Number of Principal Investigator	G.D. Robertson 456-6411, ext. 300
Short Title of Work	High-Strength Fiber-Optic Waveguide
Contract Period Covered by this Report	9 April 1978 - 31 July 1978

This research was sponsored by the Defense Advanced Research Projects Agency under ARPA Order No. 3591, Contract No. MDA 903-78-C-0289.

UNCLASSIFIED

SECURITY CLASSIFICATION OF THIS PAGE (When Data Entered)

REPORT DOCUMENTATION PAGE	READ INSTRUCTIONS BEFORE COMPLETING FORM
1. REPORT NUMBER	2. GOVT ACCESSION NO. A134931 / 3. RECIPIENT'S CATALOG NUMBER
4. TITLE (and Subtitle) HIGH-STRENGTH FIBER-OPTIC WAVEGUIDE	5. TYPE OF REPORT & PERIOD COVERED Quarterly Report No. 1 9 Apr 1978 - 31 Jul 1978
	6. PERFORMING ORG. REPORT NUMBER
7. AUTHOR(s) G.D. Robertson	8. CONTRACT OR GRANT NUMBER(s) MDA 903-78-C-0289
9. PERFORMING ORGANIZATION NAME AND ADDRESS Hughes Research Laboratories 3011 Malibu Canyon Road Malibu, CA 90265	10. PROGRAM ELEMENT, PROJECT, TASK AREA & WORK UNIT NUMBERS ARPA Order No. 3591 Program Code 8D10 Prog.Element Code 61101E
11. CONTROLLING OFFICE NAME AND ADDRESS Defense Advanced Research Projects Agency(DoD) 1400 Wilson Boulevard Arlington, VA 22209	12. REPORT DATE November 1978
	13. NUMBER OF PAGES 93
14. MONITORING AGENCY NAME & ADDRESS(if different from Controlling Office)	15. SECURITY CLASS. (of this report) UNCLASSIFIED
	15a. DECLASSIFICATION DOWNGRADING SCHEDULE

16. DISTRIBUTION STATEMENT (of this Report)

Approved for public release; distribution unlimited.

17. DISTRIBUTION STATEMENT (of the abstract entered in Block 20, if different from Report)

18. SUPPLEMENTARY NOTES

19. KEY WORDS (Continue on reverse side if necessary and identify by block number)

High-strength silica fibers
Fiber-optic waveguides
Metal-clad fibers
Static fatigue of silica

20. ABSTRACT (Continue on reverse side if necessary and identify by block number)

The objective of this program is to develop techniques leading to an optical waveguide able to withstand a continual strain of 2% for 10 years in a humid environment. The approach is to use a hermetic jacket of metal to protect the inherently strong silica fiber from static fatigue attack by moisture. The main technical problem is the application of a metal sheath free of defects over multikilometer →

DD FORM 1 JAN 73 1473 EDITION OF 1 NOV 65 IS OBSOLETE

UNCLASSIFIED

SECURITY CLASSIFICATION OF THIS PAGE (When Data Entered)

lengths without serious degradation of the initial high strength of the pristine silica waveguide.

During the first quarter, temperature control of the metal coating tip was identified as the most critical parameter in eliminating sporadic openings in the metal sheath which lead to low-strength ruptures. Toward the end of this period we produced kilometer lengths of metal-clad fiber substantially free of such defects. Evaluation studies will begin next quarter.

A research study of the inherent static fatigue resistance of silica doped with GeO_2, B_2O_3, and P_2O_5 has been initiated, ~~at UCLA~~. Development of sample preparation and testing techniques has been started and will continue into the next quarter.

Improved experimental methods for evaluating the excess optical attenuation in axially strained waveguides have been pursued. A suitable test site has been located and support equipment has been assembled for tests scheduled to begin late in the next quarter. Both metal- and plastic-clad waveguides will be investigated.

TABLE OF CONTENTS

SUMMARY

The purpose of this program is to develop and demonstrate techniques for producing multikilometer lengths of low-loss fiber-optical waveguide that is highly resistant to static fatigue. The goal is a 10-km length of waveguide which will have a 95% probability of surviving a continual 2% strain for 10 years in a humid environment. Our basic approach is to sheath the normally static-fatigue-sensitive silica waveguide with an impervious (hermetic) jacket of metal. The main problem being faced is the means for applying this jacket with true hermeticity over long lengths without degradation in the inherent high strength of the pristine silica waveguide. Efforts during the first half of the program will concentrate on the impact of metal coating technology on strength; in the second half, we will also include studies of all-synthetic glass preforms as a way to eliminate the rare flaws found in preforms made from natural quartz.

During this quarter (the first) of the program, we re-examined metal-coating process parameters and identified coating tip temperature control as the most critical in eliminating sporadic openings that destroy the hermeticity and the mechanical protection afforded the silica by the metal sheath.

A complementary research study has been initiated at UCLA into the inherent static fatigue resistance of doped silica in contrast to the already known characteristics of pure silica. This effort will use stress concentration effects at internal oblate bubble surfaces to identify any fatigue that might result from the migration or action of the multivalent cations (i.e., Ge, B, and P) used to control the refractive index in the waveguide core.

To clarify earlier preliminary measurements on changes in optical attenuation when waveguides are axially strained, a 200-m-long test site has been located and necessary measuring equipment is being assembled. By the use of optical time domain reflectometry, the central section of a strained fiber can be examined with minimal interference from the end effects, which may have affected earlier measurements.

During the next quarter, we expect to fabricate and evaluate kilometer lengths of metal-clad fiber free of openings in the metal sheath, begin the axial strain tests, finalize sample preparation and testing procedures for the oblate bubble studies, and initiate work with plastic overcoats for the metal-clad fibers to provide additional ruggedization and corrosion protection for anticipated deployment conditions.

SECTION I

INTRODUCTION

A. BACKGROUND

The goal of this program is to develop procedures for fabricating continuous 10-km lengths of low-loss fiber-optical waveguide that will exhibit survival probabilities in excess of 95% at 2% strain for 10-year service in high-humidity environments. The effort centers around a unique procedure developed at HRL for hermetically sealing the glass fiber in a metallic jacket. This hermetic jacket provides substantial protection to the glass fiber surface from the deleterious effects of moisture and other environmental contaminants which cause static fatigue (i.e., a reduction in fiber strength with time). Test results on recently prepared glass fibers evaluated in a humid environment under high stress indicate that survival times are at least five orders of magnitude longer for the Hughes aluminum-coated fibers than for state-of-the-art polymer-coated fibers.

1. Metal Coating Techniques

The application of metal sheaths to silica fiber for use in high-temperature-resistant composite systems was pioneered in the mid-1960s by Rolls-Royce Ltd. In this work, the metal coating was applied by the freeze method shown in Figure 1. Because of the generally satisfactory coating results and the ready adaptability of this method to high-volume production, we have continued to use this technique for the coating of optical waveguides and fibers. Figure 2 shows the essential details of the coating apparatus, which incorporates a reservoir for the molten metal connected by a delivery tube to an annular tip. A bead of the molten metal is held in the center of the hot annular tip by surface tension. As the fiber passes freely through the bead, a layer of metal freezes to the glass surface and is carried out of the bead. Molten metal from the reservoir replenishes the material as it is consumed. To prevent an oxide scum from developing on the surface of the molten

5332 10

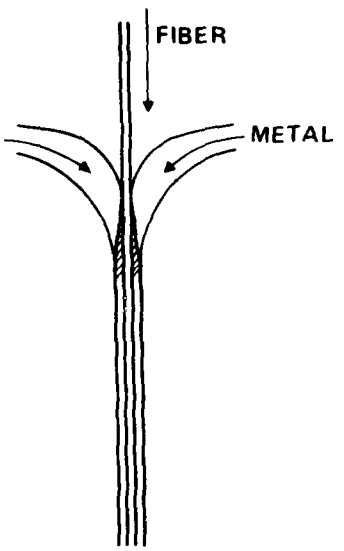

CONTROL PARAMETERS

TEMPERATURE OF METAL BATH

TEMPERATURE OF FIBER

FIBER SPEED

ATMOSPHERE

Figure 1. Schematic of metal freeze coating process. With proper control of parameters such as fiber speed and temperature, metal bath temperature, and surrounding atmosphere, a smooth metal jacket freezes around the fiber.

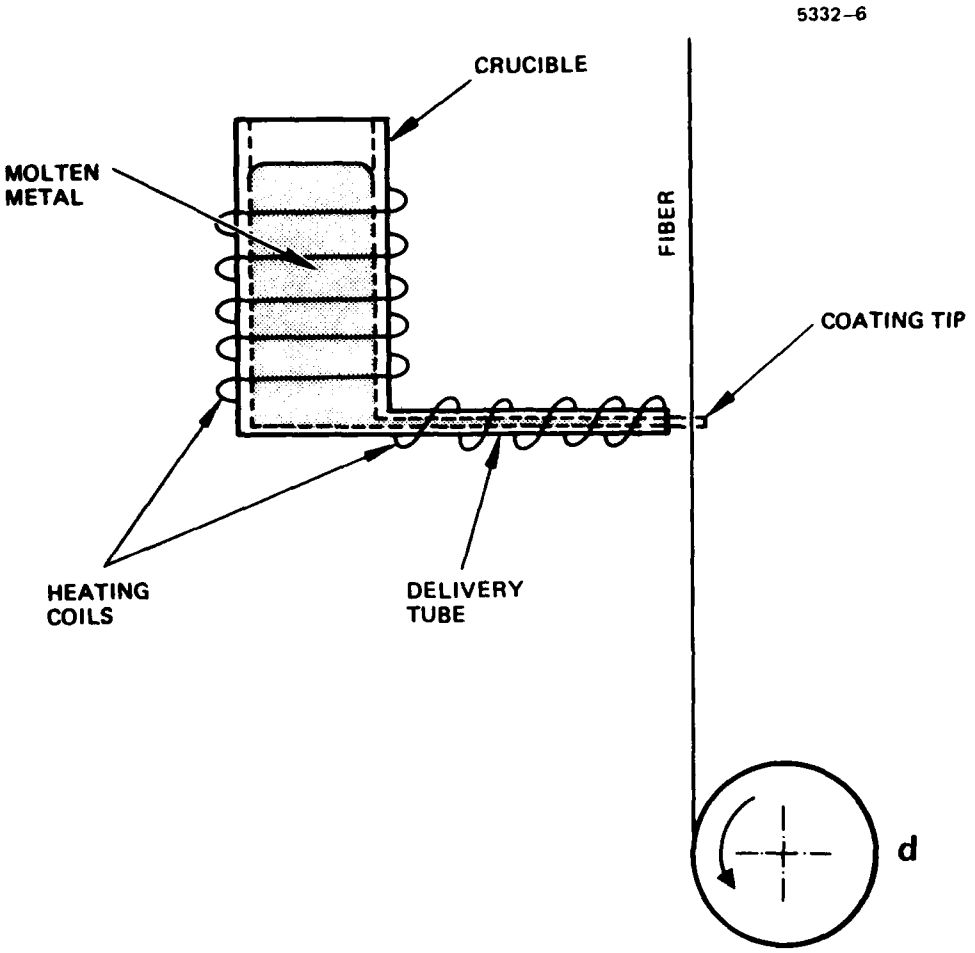

Figure 2. Metal coating apparatus. Fiber speeds in excess of 2 m/sec can be accommodated in this type of coater.

metal, gas-composition control is provided for both the entrance and exit surfaces of the molten-metal bead.

We have been working for about 2 years with this technique and have made great strides in achieving coating-thickness control and structural integrity in the metal film, which must provide a hermetic seal to protect the silica surface from any contact with ambient moisture or other contaminants. Coating rates between 1 and 2 msec are readily attained. Such rates are commercially attractive for fiber manufacturing. Our main efforts recently have been directed toward certain details of the coating operation that now appear to require more precise control than had been previously realized. When all of the process parameters are set at proper levels, the surface of the metal coating is smooth and uniform, as shown in Figure 3.

In cross section, the coating has the appearance shown in Figure 4(a) and (b) for two different waveguide samples. The fiber diameters here are about 100 μm, and the aluminum coating usually varies between 15 and 20 μm in thickness. Normally, the coating is symmetric about the fiber, as seen in Figure 4(a), but occasionally it will show a slight asymmetry of the magnitude seen in Figure 4(b). If the asymmetry increases much beyond that shown, the coating conditions are not being properly controlled and the coating is usually not continuous.

If all parameters are not properly set, then various kinds of localized defects appear. From the standpoint of strength degradation, the worst defect probably is an opening, or pinhole, in the metal sheath. Figure 5 shows a region in which the metal appears not to wet the silica surface. This is usually attributed to operation of the metal coating tip at a temperature slightly above the optimum value. During proof testing or subsequent use, the uncovered surface area is subject to mechanical abrasion (if it is large enough to allow penetration by foreign objects) and to stress corrosion by water, leading to reduced ultimate strength (static fatigue).

Another type of defect that occurs is the circumferential hillock visible in Figure 6. It has the appearance of a joint in a bamboo stalk and is caused by a momentary thicknening of the applied coating.

7894-3

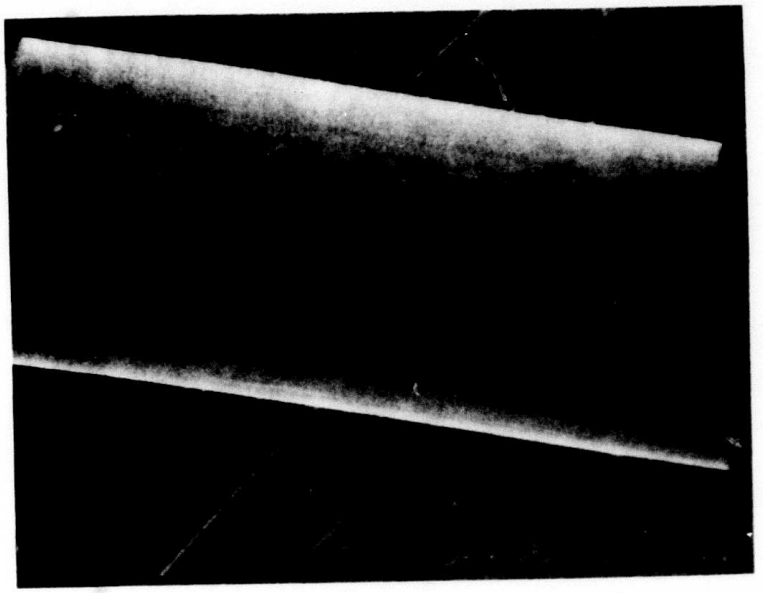

(a) Aluminum jacket

6857-13

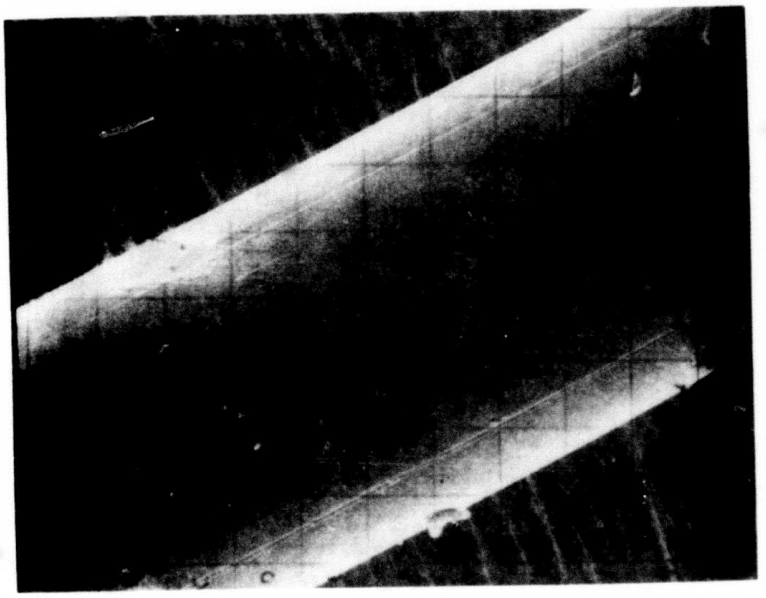

(b) Tin jacket

Figure 3. SEM photographs of high-quality metal jackets. In these 300x enlargements, the smooth metal surface achieved when all coating parameters are under control is visible.

5872-16

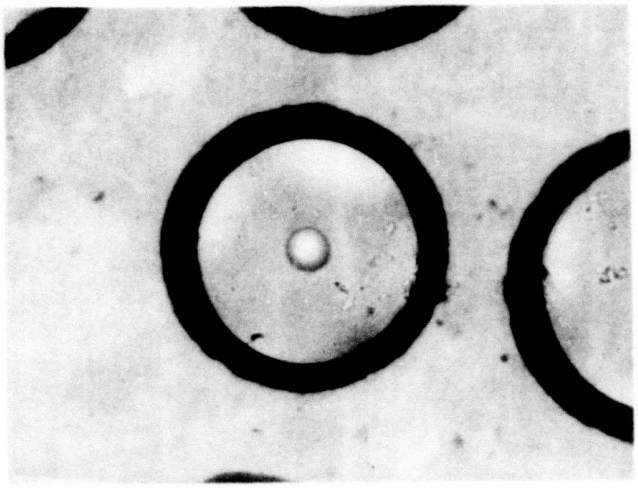

(a) The metal jacket is the dark ring of about 20 μm thickness surrounding the 100-μm-diameter graded-index waveguide.

6725-5

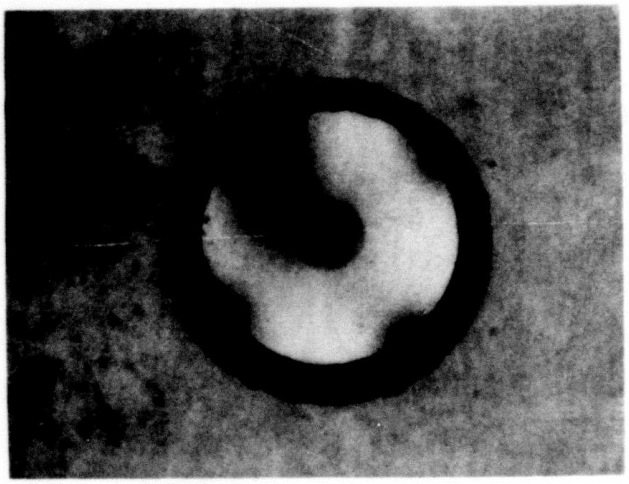

(b) This step-index waveguide has a diameter of 115 μm and an aluminum jacket with slightly varying thickness.

Figure 4. Thin section photographs of aluminum-jacketed waveguides seen with transmitted light.

7894-10

Figure 5. Poorly coated sections of aluminum-clad SiO_2. In this 300x SEM photograph, a portion of the SiO_2 surface is not wetted by the Al jacket. Analysis by energy dispersive x-ray analysis (EDAX) shows only Si in the open area; we have not found any contaminating species to be the cause for these random openings. (300x).

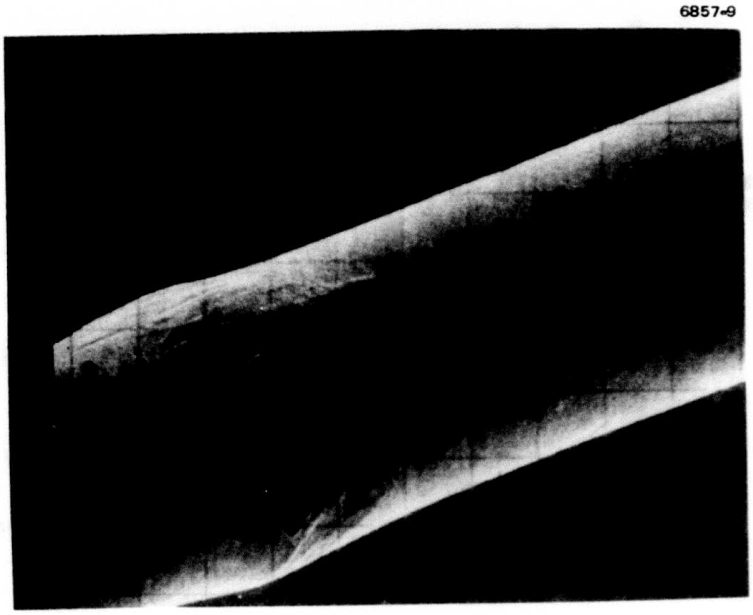

Figure 6. Circumferential hillock in aluminum jacket. This localized thickening in an otherwise smooth metal jacket has the appearance of a joint in a bamboo stalk. (300x)

Such features result when the metal coating tip is operated slightly below the optimum temperature. This perturbation does not appear to adversely affect fiber strength, but we recently determined that it is a source of microbending when the waveguide is in contact with a surface, such as when the waveguide is wrapped on a drum or a payout spool. Although the effects from any one such hillock may be slight, they often occur periodically at relatively close spacing, as seen at the locations of the arrows in Figure 7. In this case, the hillocks are only about 0.6 mm apart and could thus cause 1600 microbends/m.

6857-10

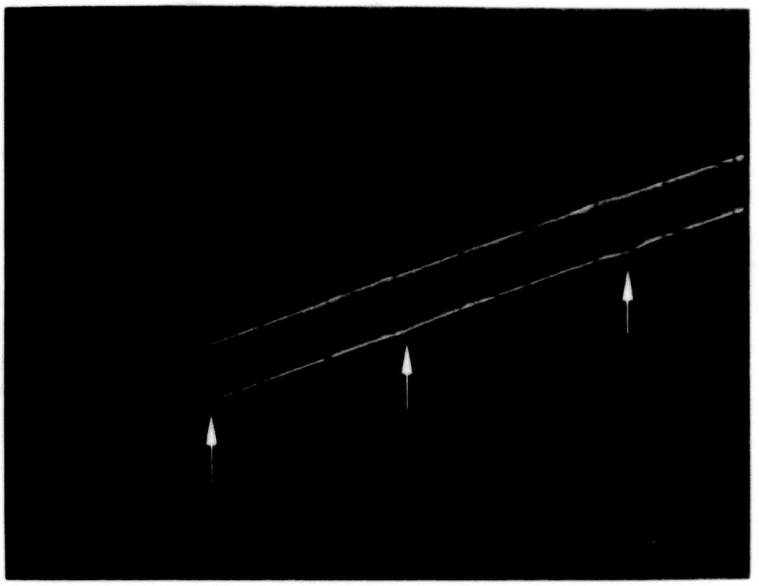

Figure 7. Periodically spaced hillocks in an aluminum jacket. The regular occurrence of hillocks, separated by 0.6 mm (as shown by the arrows), is a likely cause for microbends in a waveguide.

Although these various types of defects are extreme examples of coating perturbations, they must be prevented in long lengths of fiber intended to be stressed in use. Even one opening of the type shown in Figure 5 would be disastrous in a fiber-payout system. Careful monitoring and control is needed of parameters such as fiber diameter and speed, cleanliness of the fiber surface at the time of entry into the molten metal, composition of the gas above the metal entrance surface, impurity content of the liquid metal, gas composition at the exit surface from the metal, length of the coating region, and particularly the temperature and temperature gradients. Careful adjustment and optimization of each of these parameters appears essential to achieving a good coating with consistently high quality over multikilometer continuous lengths. Although we have made substantial progress towards achieving such high-quality fiber, much careful work remains to be done before all key parameters are identified, controlled, and their mutual interactions understood.

2. Dynamic Strength

The response of a fiber-optical waveguide to dynamic stresses is an important consideration in many field applications. These stresses may arise during deployment as well as afterwards from operational loading. The effects of static loads, experienced either in storage or in use, are discussed below. It is well known that the observed tensile strength of glass fibers exposed to a humid atmosphere depends on the rate at which stress is applied. Because it is more convenient to consider the strain resulting from the applied stress, the dynamic strength of glass is usually expressed as a function of strain rate. Some strength data obtained by several investigators for silica glasses at a variety of strain rates are listed in Table 1. The trend line from Proctor's data is plotted in Figure 8. The faster the load is applied, the stronger the glass fiber appears to be. The data provide a boundary between regions of safe operation and failure. Because of this strain-rate effect, it has become a commonly accepted practice to test glass fibers at a strain rate of 20% per minute. This value represents a

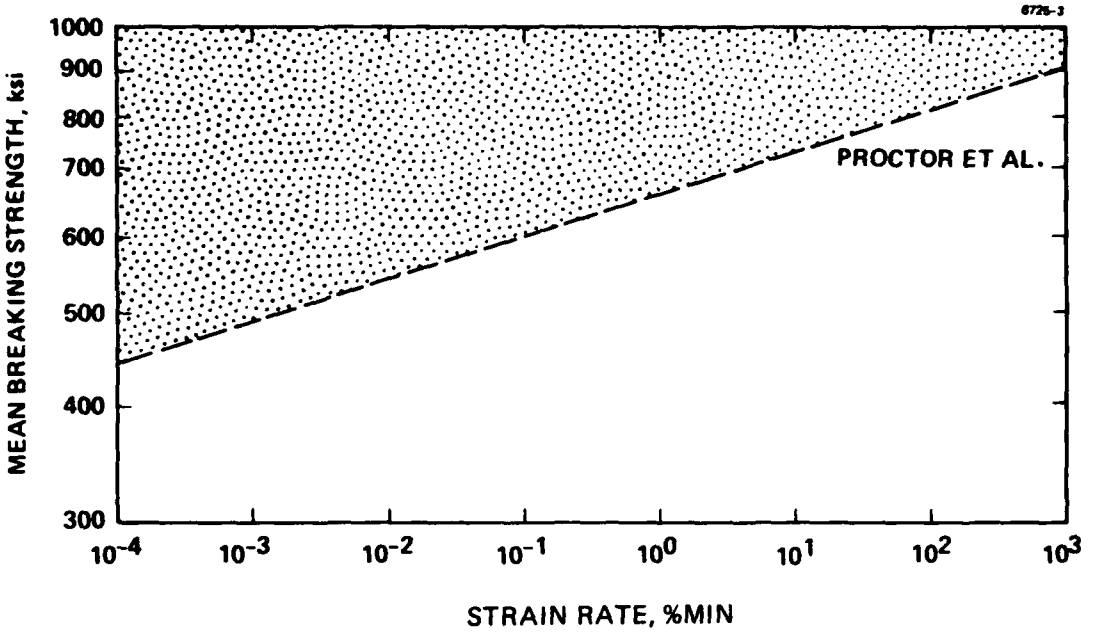

Figure 8. Published dynamic fatigue data for SiO_2. Unprotected and plastic coated silica fibers exhibit an increase in strength when tested rapidly because of the reduced impact of static fatigue during the correspondingly shorter test period.

B.A. Proctor, L. Whitney, and J.W. Johnson, Proc. Roy. Soc. 297A, 534 (1967).

Table 1. Mean Breaking Strength of Bare or Plastic-Clad Silica Fibers

Strain Rate, %/Min	Mean Breaking Strength, kpsi	
	Bare Vitreosil[a]	Plastic-Clad TO-8 Silica[b]
0.4	590	390
4.0	685	480
20.0	750	550
80.0	815	610

[a] 5-cm gauge length, 25-μm-diameter Vitreosil fiber. B.A. Proctor, L. Whitney, and J.W. Johnson, Proc. Roy. Soc. 297A, 534 (1967).

[b] ∿4-cm gauge length, 100-μm-diameter TO-8 fiber. Krause and Kurkjian, Paper TuA 3, Optical Fiber Transmission II, Williamsburg, VA, 22-24 Feb 1977.

6376

compromise between testing convenience (short time per test) and a variety of applications for which strain rates may be much lower. As the strain rate decreases, the test values approach those obtained from "static fatigue" tests (as discussed below). However, since acquiring static fatigue results often takes too long, dynamic strength tests are used. Recently, Ritter[1] and others have proposed the use of dynamic testing techniques for approximating the long-term static fatigue behavior of glass fibers. Although the data available to test this proposal are still meager, it appears that valuable system-design data on long-term behavior can be obtained from short-term data obtained over a variety of strain rates.

[1] J.E. Ritter, Jr., "Engineering Design and Fatigue Failure of Fused Silica Fibers," Fracture 1977, Vol. 3, ICF4, Waterloo, Canada, June 19-24, 1977.

We recently examined the tensile strength of metal-coated silica glass fibers over a wide range of strain rates. The objective was to compare their performance with that of plastic-clad and bare silica fibers. We discovered that the response of metal-clad fibers to strain rate is strikingly different from that of conventional silica fibers. We believe that this difference will remove many of the design restrictions that are currently imposed on the use of optical waveguides in potentially high-stress applications.

These recent data were obtained by conventional tensile testing in an Instron Universal Tester at strain rates ranging from a high of 80%/min (the maximum possible with this test machine) to a low of 0.04%/min (the limit being set by the length of time for which the tester could be devoted to these measurements). The time required to rupture each specimen varies correspondingly from a few seconds to several hours. The gauge sections were 12.5-cm long, which is about 2 to 3 times longer than those used to obtain the data in Table 1 and Figure 8.

We found that the tensile strength of the metal-coated glass is independent of the strain rate at which it is tested. Table 2 presents the results of these tests, and Figure 9 shows these data superimposed on the results for conventional fibers from Figure 8; data from Ref. 1 is also included. The mean breaking stress for each group of 25 samples is plotted along with vertical bars representing the standard deviation. In addition, some individual datum points at the extreme of the high strength distribution have been plotted to emphasize their deep penetration into the failure region. In spite of the rather large spread in the strength at each test condition, the main breaking strengths of the fibers are completely independent of the strain rate imposed during the tensile test. Thus, for this type of fiber, it makes no real difference how quickly or slowly the load is applied. Such behavior implies that

---

[1] Krause and Kurkjian, Paper TuA 3, Optical Fiber Transmission II, Williamsburg, VA, 22-24 Feb 1977.

Table 2. Tensile Strength of Metal-Coated Fibers at Different Strain Rates

Strain Rate, %/Min	Tensile Strength, kpsi		
	Maximum	Minimum	Average ± Std. Dev.
0.04	929	373	515 ± 156
0.4	695	300	511 ± 106
4.0	697	367	519 ± 92
20.0	736	315	529 ± 97
40.0	761	379	498 ± 106
80.0	667	305	515 ± 88

Gauge length = 12.5 cm.

Sample size = 25 specimens per strain rate condition.

Tests at 0.04 and 40%/min strain rates are from one fiber and the remainder are from a different fiber.

the strength of such fibers in use does not have to be derated for long-term exposure or high-stress levels.

The currently accepted explanation for the dynamic behavior of conventional silica fibers is based on the stress corrosion induced by moisture at flaw sites located at the surface of the glass fiber. This same phenomenon acting on a much longer time scale is also invoked to explain static fatigue. The good correlation found by Ritter[1] is accepted as evidence that the same mechanism of strength reduction is at work in both the dynamic and static regimes. On the basis of our observations of the stability of the strength of metal-coated silica over a wide range of strain rates, one would expect static fatigue to be absent

[1] J.E. Ritter, Jr., "Engineering Design and Fatigue Failure of Fused Silica Fibers," Fracture 1977 Vol. 3 ICF4, Waterloo, Canada, June 19-24, 1977.

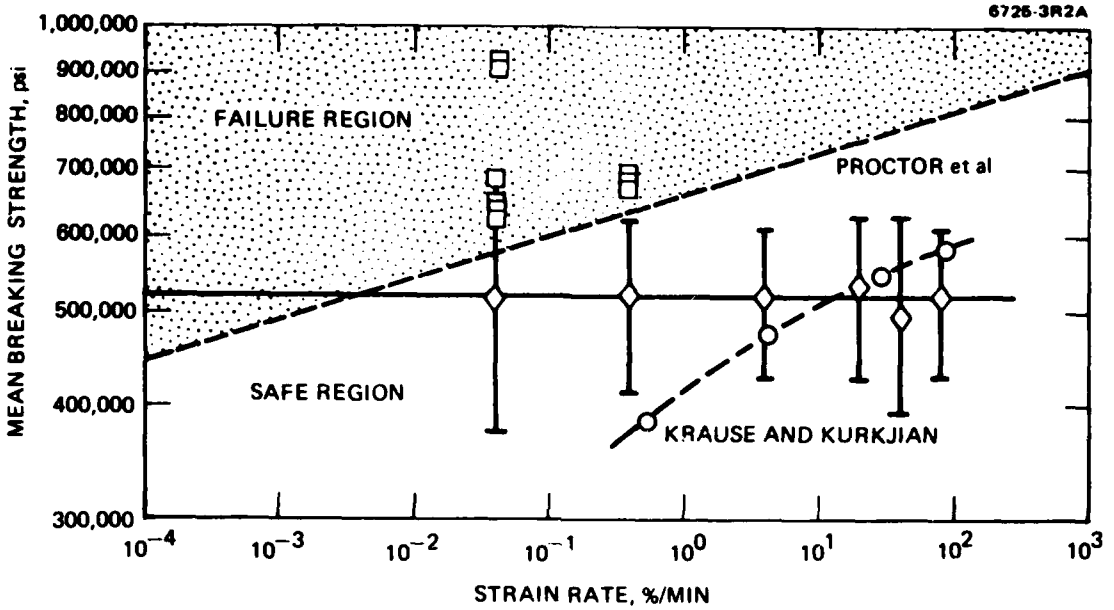

Figure 9. Strength of metal-coated fibers at various strain rates. The average strength of the metal-coated fibers is independent of the strain rate and several individual samples were found to exhibit strengths in the region forbidden by fatigue effects. (B.A. Proctor, L. Whitney, and J.W. Johnson, Proc. Roy. Soc. 297A, 534 (1967)) (J.T. Krause and C.R. Kurkjian, Paper TUA3, Optical Fiber Transmission II, Williamsburg, A., 22-24 February 1977).

from metal-coated silica fibers. Although it takes a long time to collect such data, especially at moderate stresses (300 to 500 kpsi), results discussed below indicate that the expectation is correct.

For each of the data sets listed in Table 2, a sample population of 25 specimens was tested. When the data are treated by the method of Weibull,[1] the strength distribution can be interpreted in terms of a cumulative failure probability for the population from which the sample was obtained. Although there is no a priori justification for this treatment, it is a convenient choice among the several extreme-value statistical models that must be applied to a material with flaw sites randomly distributed both in size and frequency of occurrence. If sufficient data are collected to define the modal distributions of flaw sizes, then a Weibull plot permits calculating failure-strength probabilities as a function of gauge length.

A Weibull plot of the metal-coated data presented in Table 2 and Figure 9 is given in Figure 10 for the lowest strain rate. It is interesting that two of the specimens did not fail until the stress reached a value in excess of 900 kpsi. On the basis of short-term static fatigue, the lifetime of a silica fiber at 700 kpsi is about 1 sec. The extrapolated lifetime at 900 kpsi is less than 10 msec. However, the two highest-strength specimens in Figure 10 were exposed to stresses above 700 kpsi for more than 50 min (3000 times the expected life of a plastic-clad fiber). It appears that the potential for producing really strong fibers of high durability is outstanding for the metal-clad silica system.

3. Static Fatigue

It is now well known that glass fibers typically exhibit a high tensile strength when they are subjected to a brief loading, such as a jerk, rather than a continuous applied load. This phenomenon, which is

[1] W. Weibull, "A Statistical Distribution Function of Wide Applicability," J. Appl. Mech. 18, 293-297 (1951).

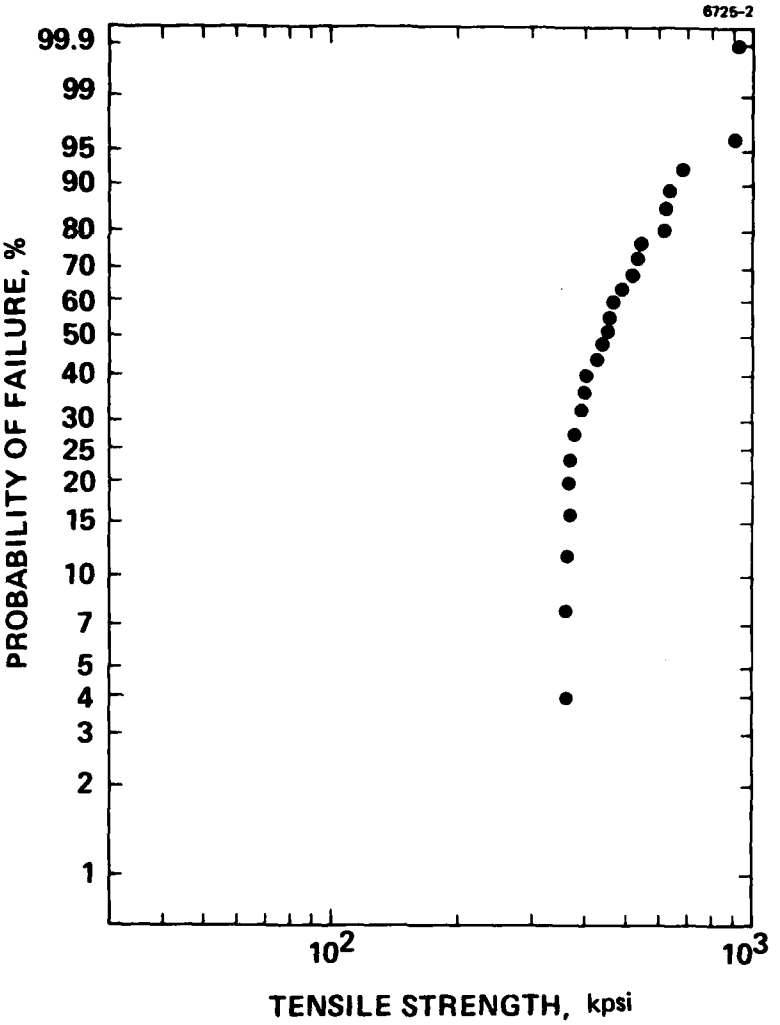

Figure 10. Weibull-type plot of strength data obtained at a strain rate of 0.04%/min. The key feature of this plot is the survival of the two strongest specimens (gauge length is 12.5 cm) for a time of more than 50 min at a stress level above 700 kpsi. If static fatigue were at work, these samples would have failed in less than 1 sec.

unique to glass, was first observed at the turn of the century by Grenet[1] and has been given the name of "static fatigue" to emphasize that a fiber that does not break shortly after a load is applied may still break at some later time if the load is not removed. The microscopic origin of static fatigue in silica is not yet fully understood. However, it is known to be a form of stress-corrosion cracking somewhat like that which causes stainless steel to crack in the presence of the chlorides found in salt water. In the case of silica, the principal agent contributing to stress-corrosion cracking or fatigue is known to be moisture. Other mobile impurities such as sodium ions, which are surprisingly mobile and ubiquitous, can also contribute to failure. Cox[2] has proposed a semi-quantitative microscopic model to explain static fatigue. According to this model (which is depicted in Figure 11), an Si-O bond may occasionally break in the silica structure when several phonons randomly localize and provide sufficient energy to ionize the bond. Because of the brief lifetime of a phonon, this condition will only last for about 10^{-12} sec. The Si-O bond will usually reform since each Si atom is held rigidly in place by four oxygen bonds, and it is likely that only one will break at a time. The three remaining bonds will prevent any physical separation that might otherwise cause the broken bond to remain permanently open. However, if some mobile impurity such as H_2O is in the vicinity of an Si-O bond on the surface of the fiber during the instant the bond is ionized, it is probable that the H_2O will chemically react with the ionized silicon and oxygen, resulting in a permanent failure of the Si-O bond. This failure is the nucleus for further flaw growth since the applied stress will open the first broken bond and expose the Si-O bonds below it to water molecules. The flaw will continue to grow as this process is repeated unless the water is completely eliminated.

---

[1] Luis Grenet, Bull. Soc. Enc. Industr. Nat. Paris (Series 5), Vol. 4, p. 838 (1899).

[2] S.M. Cox, Phys. Chem. Glasses, Vol. 10, p. 226 (1969).

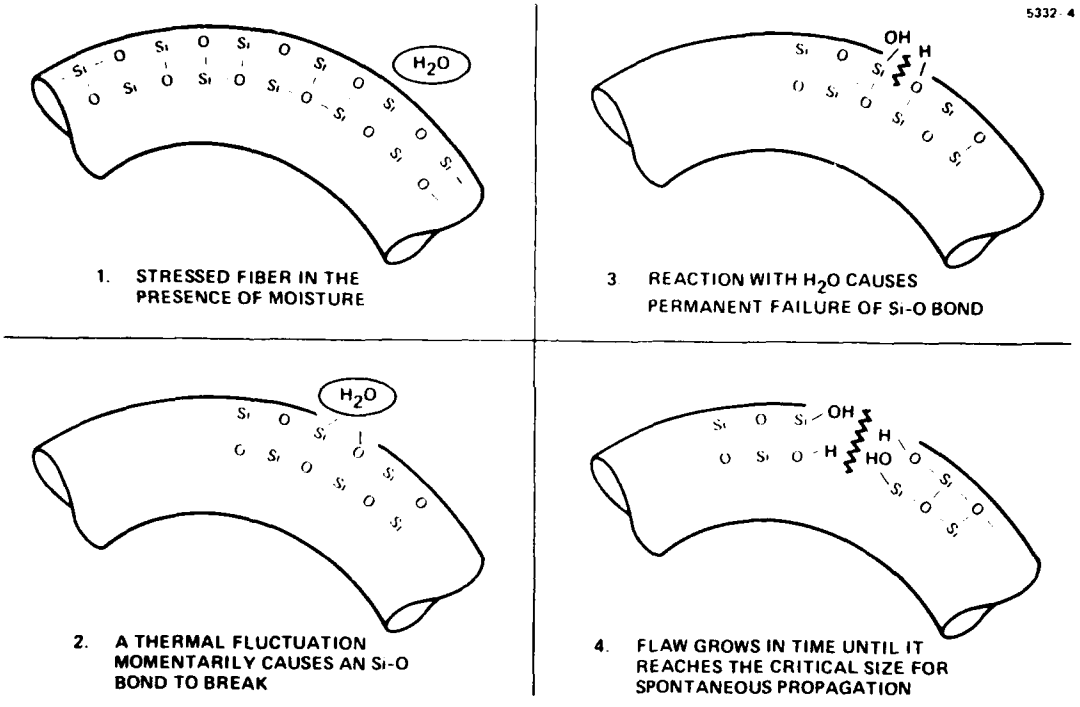

Figure 11. Qualitative model for fatigue in silica. The progressive failure of Si-O bonds in the presence of moisture accounts for both dynamic and static fatigue observation in unprotected and plastic-coated fibers.

An interesting feature of this model is that it can be used to unify both the dynamic and static fatigue mechanisms. In dynamic fatigue, as discussed in the previous section, the failure load depends on the rate at which a fiber is strained. Conventional static-fatigue test results are obtained by observing the time to failure of a sample held at a constant value of applied stress. The origin of both dynamic and static fatigue is the microscopic growth of flaws such as depicted in Figure 11. However, if a monotonically increasing load is applied faster than fatigue cracks can grow, the fiber will appear to have extra strength. Since this additional strength is a very fleeting commodity, all strength comparisons of fibers should be made at comparable, well-controlled values of strain rate. The only real difference between dynamic and static fatigue is in the rate of loading. In dynamic fatigue studies, the load is usually applied faster than the crack growth rate, while the opposite is true in static-fatigue experiments.

Based on the above model, it becomes obvious that if moisture and other harmful contaminants could be eliminated from the fiber surface by a hermetic jacket, then fatigue could, in principle, be eliminated. Over the past 18 months, we have accumulated an impressive amount of data to verify that this is the case for pure silica fibers. Figure 12 summarizes all of the known static-fatigue data on unprotected and plastic-coated silica fibers made in England,[1] the United States,[2] and Japan.[3] The safe and failure zones are reasonably similar with the deviations attributable to differences in initial flaw distributions. Larger initial flaws will certainly lead to early failure since less fatigue growth is required before the crack reaches the critical size for spontaneous propagation. Also shown in Figure 12 are datum points for metal-coated fibers made at HRL which continue to survive for times

---

[1] B.A. Proctor, I. Whitney, J.W. Johnson, Proc. Roy. Soc., Vol. 297A, p. 534 (1967).

[2] C.K. Kao, M. Maklad, and V. Schurr, Topical Meeting on Optical Fiber Transmission I, February 22-27, 1977, Williamsburg, Va., Paper TUA6.

[3] T. Kobayashi, et al., Paper B9-4, IOOC 1977, Fujihuma, Tokyo, 22-24 July 1977.

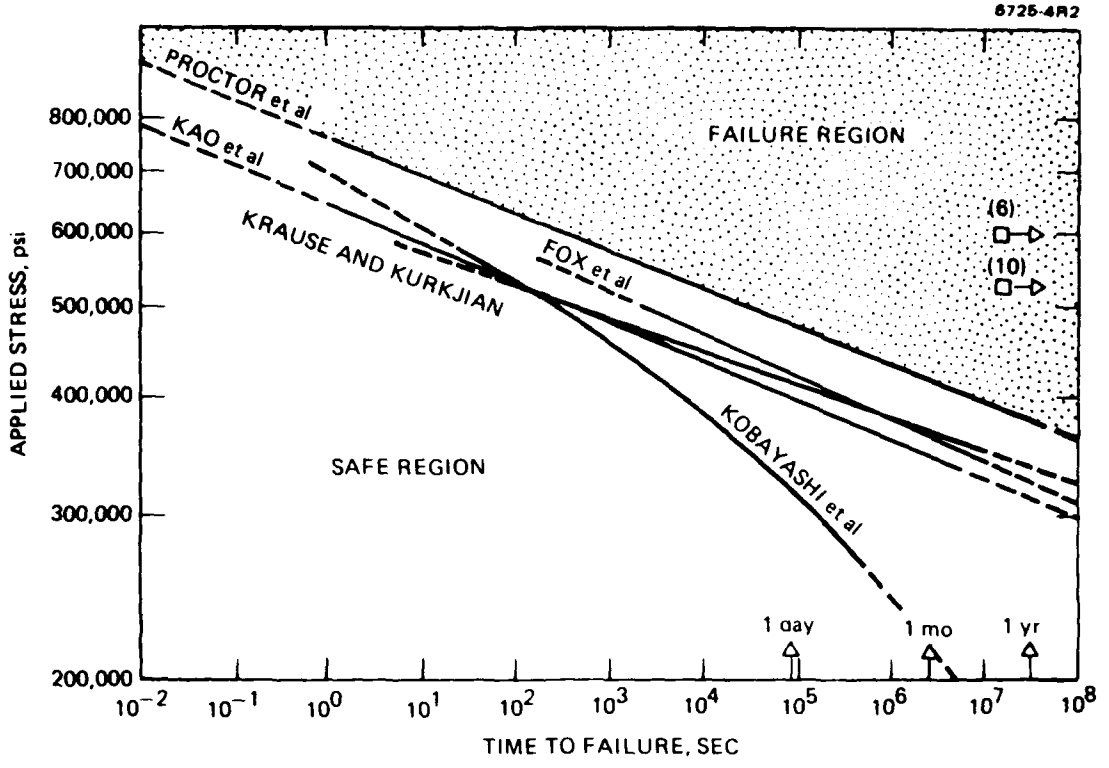

Figure 12. Static fatigue data for silica. These data are representative of results obtained in the United States, England, and Japan during the past 10 years. The two squares represent HRL metal-jacketed fibers still being tested.

B.A. Proctor, L. Whitney, J.W. Johnson, Proc. Roy. Soc., Vol. 297A, p. 534 (1967).

C.K. Kao, M. Maklad, and V. Schurr, Topical Meeting on Optical Fiber Transmission II, February 22-27, 1977, Williamsburg, Va., Paper TUA6.

T. Kobayashi, et al., Paper B9-4, 100C '77, Fujihuma, Tokyo, 22-24 July 1977.

J.T. Krause and C.R. Kurkjian, Paper TUA3, Optical Fiber Transmission II, Williamsburg, A., 22-24 February 1977.

in excess of five orders of magnitude longer than the plastic-clad fibers. Even more impressive is the fact that some of the HRL fibers have been immersed in tap water for the entire duration of the test, which is still continuing. Clearly, the hermetically protected fibers have far superior survival characteristics in air and under water.

There has been some confusion about the validity of Cox's microscopic model for static fatigue of silica, which requires the presence of moisture as an essential ingredient for fatigue failure. This is because the literature is full of data indicating that fatigue can proceed in glass even in the absence of external moisture. But there is really no contradiction. All of the data describing fatigue in the absence of moisture is for "soft" glasses such as soda lime silica rather than pure silica. Even without the presence of moisture, soft composite glasses are subject to fatigue by an additional mechanism, the mobility of cations such as Na^{+}, which allows them to preferentially migrate to crack tips and accelerate failure. Qualitatively, the monovalent ions, when concentrated in the crack tip, reduce the strength because their single bonds cannot contribute to the cohesive three-dimensional bridging structure of the host glass. Work on composite glasses, including fiberglass, suggests that monovalent cations are the principal troublemakers for static-fatigue failure, while divalent and higher valency cations are thought to be locked firmly into the host structure by their multiple bonds. It is interesting that, after many years of development, the standard fiberglass composition (E-glass and S-glass) have evolved with no monovalent cations.

It is quite fortunate that the dopants commonly added to silica to make low-loss waveguides, such as B^{3+}, P^{5+}, and Ge^{4+}, are all multivalent and are not expected to contribute to static fatigue. This tentative conclusion requires experimental verification, and a research effort to do this has been initiated as part of this program.

Another concern is that static fatigue in pure silica can proceed not only by external moisture contamination, but also by the moisture known to be incorporated in the silica structure when it is initially formed. Most of our test fibers have been drawn from Suprasil II, a

synthetic silica made by burning $SiCl_4$ in an oxyhydrogen flame. Silica produced in this fashion is known to contain approximately 1200 parts per million of water entrapped in the silica host. Based on our experimental results, we can conclude that this water is quite immobile at ambient temperatures. Otherwise, we would not have achieved such excellent results. However, the possibility exists that the entrapped water has a very low mobility and will eventually limit fiber lifetime. Whether this is the case or not should not be significant since we plan in the future to make preforms entirely by the chemical-vapor deposition (CVD) method. In this case, the silica is formed by the endothermic reaction of $SiCl_4$ with pure O_2, and the resulting glass is very "dry." Typical water impurity levels are reduced by two to three orders of magnitude using CVD rather than flame hydrolysis. With additional care, even greater reductions in water impurity have been demonstrated. Thus, we presume that future fiber waveguides will not be troubled by internal moisture impurities.

4. Proof Testing

The strength data obtained on short lengths of individual fibers is generally incorporated in a Weibull plot to determine a statistical probability of failure at some strength. However, data collected from short samples cannot predict where along the axis of a long fiber any low-strength portion may occur, nor does it predict accurately what the lowest strength may be. Consequently, some type of proof testing of the fiber in long lengths is required. Two approaches may be used:

- Stretching of individual long lengths
- Drum-to-drum respooling with a short section between the drums under the proof tension.

We have taken the second method as the more practical and easily implementable technique. At HRL we use a simple technique in which two drums are turned in unison, one taking up the fiber from the other. The fiber hangs in a loop between the drums. A Teflon wheel with a known weight attached to it is placed in the loop. As the drums are rotated,

the fiber passes from the full drum under the weighted wheel onto the take-up drum. The complete length of fiber is thus passed from one drum to the other. When a break occurs, the turn number is noted, and the location of the break is recorded on a graph for the particular stress being applied. The fiber is run back and forth from drum to drum with an increased stress being applied each time. This apparatus is shown in Figure 13.

Because of the loads associated with tests of fibers having outside diameters between 150 and 200 μm, the laboratory type of apparatus seen in Figure 13 is limited to an upper stress value of about 200 kpsi. For tests at higher stress levels, more sophisticated equipment is required. For many years, proof testing of steel guidance wire for the TOW missile has been conducted by the Hughes Missile Manufacturing Division at Tucson, Arizona. One of their automated proof testing machines has been modified by changing the input/output feed spools and the tensioning reels to accept metal-clad silica fibers. With this apparatus (shown in Figure 14), long lengths of fiber can be proof tested to high stress levels (>500 kpsi). We expect to use this proof tester for further tests on long samples that have not broken up to the limits imposed by the laboratory apparatus.

5. Cyclic Loading Considerations

Since demonstrating the value of hermetic metal layers for prolonging the fatigue lifetime of silica fibers, we have turned our attention to defining the preferred metal for fiber protection. Early in the program, we had selected aluminum, tin, and indium as preferred candidates based on chemical reactivity studies and the desire for a relatively soft material, which was expected to minimize excess fiber loss caused by microbending. The majority of our coating work to date has been conducted with five-nines-pure aluminum because we were guided by the earlier work of Arridge.[1] However, we have now gained enough

[1] R.G.C. Arridge, "The Coating of Glass Fibers with Molten Metal," presented at the symposium on the contact of hot glass with metal, Scheveningen, 26-29 May 1964.

M12593

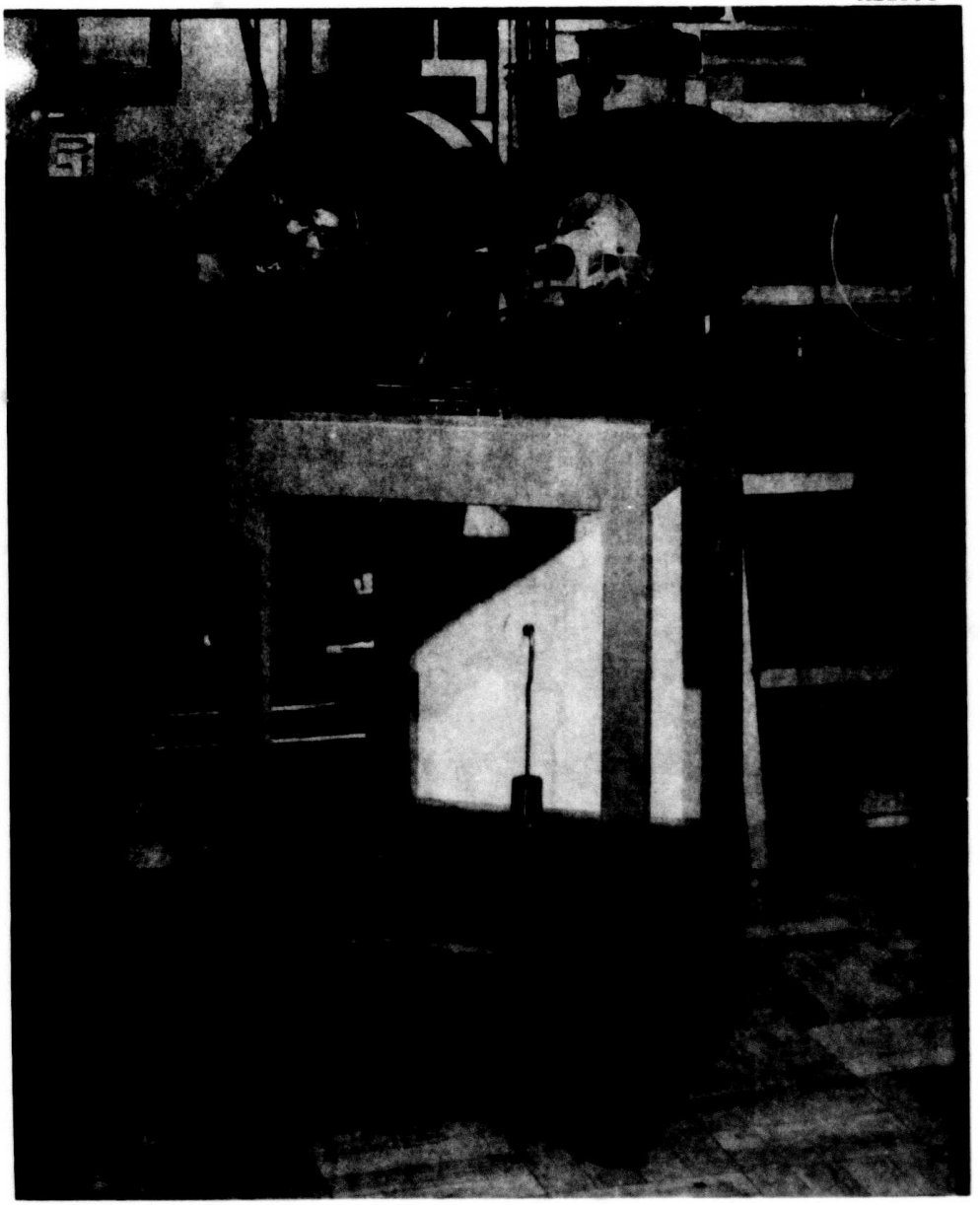

Figure 13. Continuous tensile test apparatus for laboratory use. This device allows quick testing of both short (~200 m) and multikilometer lengths of fiber up to stresses of about 200 kpsi.

5992-5

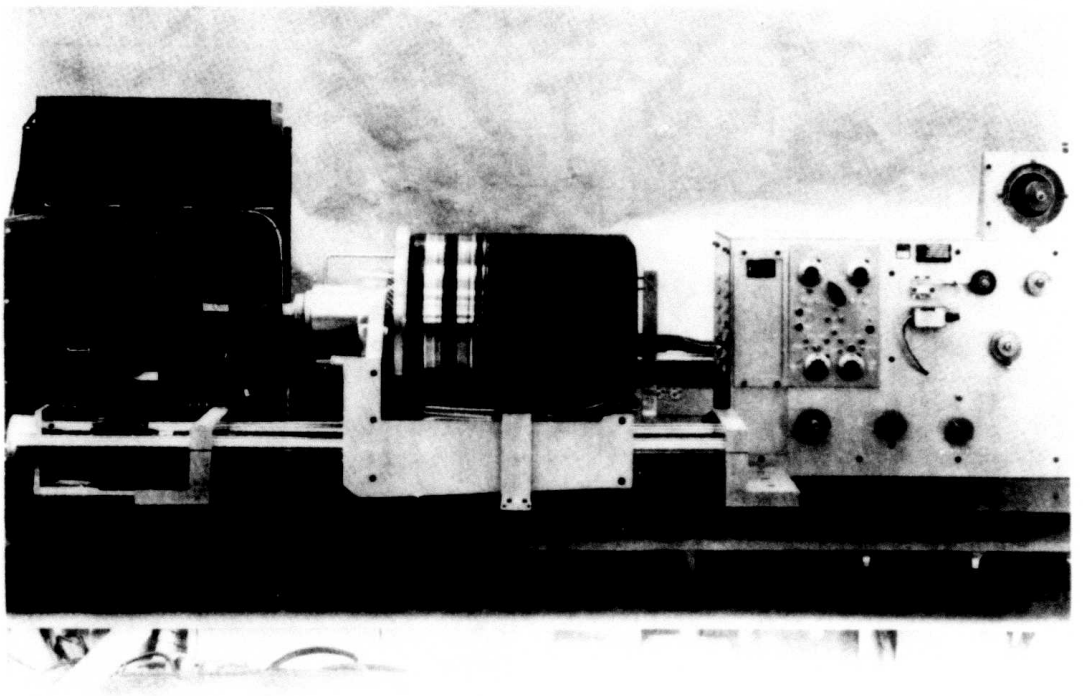

Figure 14. Automatic continuous tensile test machine. Overall view of modified continuous tensile test machine showing fiber pay-out drum. The similar take-up drum is immediately behind this drum.

experience with other metals, including tin and indium, to be confident that our existing equipment and application procedures can be adapted to them in a straightforward fashion.

A significant factor in selecting a preferred metal is the cyclic fatigue behavior of the thin metal jacket on the fiber waveguide. We have conducted tests on some of our aluminum-coated fibers to investigate whether there are important differences between the cyclic fatigue data reported in the literature for bulk aluminum[1] and our thin aluminum-coated fibers. Testing was performed on 0.5-m lengths of fibers using our Instron machine, which was programmed to alternate the stress from zero to 400,000 psi in 1-min intervals. At the 400,000 psi level, the strain in the aluminum was 4%.

According to the classical work of Coffin[1] on low-cycle fatigue in metals, the number of cycles to failure, N, is expected to be related to the alternating strain $\Delta\varepsilon$ by what is known as Coffin's empirical law:

$$N = \frac{\text{constant}}{(\Delta\varepsilon)^2} \quad .$$

The constant of proportionality can be determined simply by measuring the strain $\Delta\varepsilon$ to failure for a monotonically increasing load. Figure 15, taken from Coffin's work, shows the cyclic fatigue characteristics of bulk aluminum. From this figure, it can be established that a 4% strain level failure can be expected in several hundred cycles. Test results on the fibers ranged from approximately 100 to 250 cycles to failure. This establishes an important link between a well known body of data on bulk metals and heretofore unknown properties of the thin metallic layers used on fiber waveguides. Clearly, additional testing at other strain levels will be required. However, we have concluded that the thin metal layers behave qualitatively similar to bulk metals when they are strained. Since we were interested in observing in detail the progressive failure

[1] L.L. Coffin, Jr., Eng. Quarterly, "Metals," Vol. 3, pp. 15-24, November 1963.

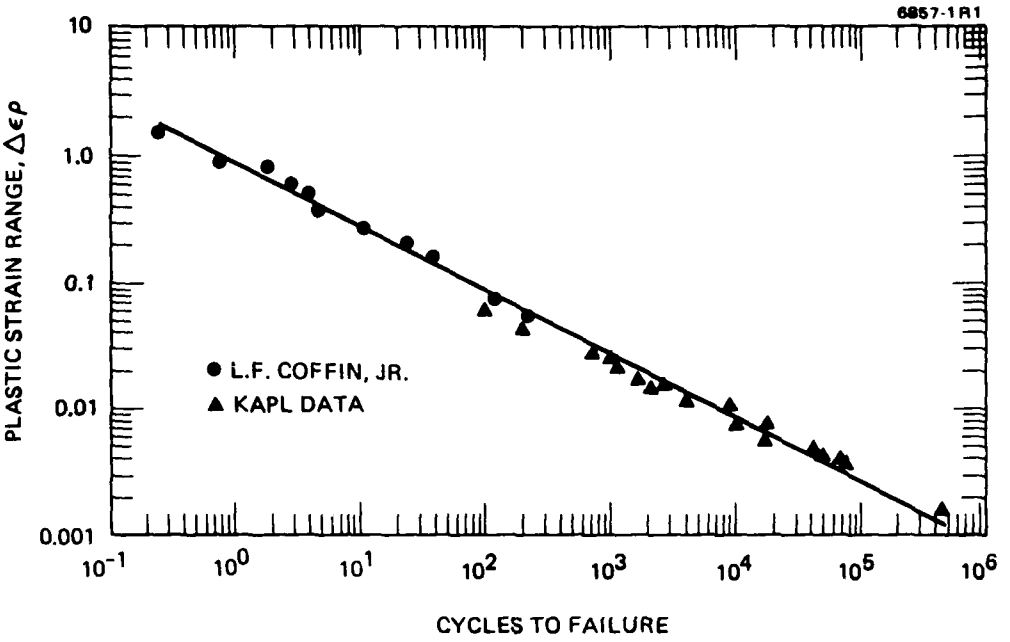

Figure 15. Plastic strain range versus cycles to failure for annealed 2S aluminum. (Adapted from L.F. Coffin, Jr., Eng. Quarterly "Metals" Vol. 3, pp. 15-24, Nov. 1963). This curve allows predicting low cycle fatigue failure in pure bulk aluminum as a function of the extent of plastic strain.

of the aluminum coatings, we made SEM photographs of the aluminized surface of the fiber before cyclic loading, after 20 cycles, and again after 250 cycles. These results are shown in Figure 16, where one can observe that slip planes develop and enlarge during cyclic loading.

Based on these results, we believe that it will be highly desirable to consider selecting a coating metal that has a low recrystallization temperature, preferably below room temperature. With such a coating, the strained metal would spontaneously recrystallize after straining, which would, hopefully, suppress the progressive crack growth that can destroy the hermetic seal. Table 3 is a tabulation of the recrystallization temperatures of selected metals taken from the American Society of Metals Handbook. The recrystallization temperature of aluminum is approximately 300°F, while both tin and lead recrystallize below room temperature. Thus, both tin and lead, as well as tin-lead alloys, should be considered as strong candidate metals for fiber coating. To date, we have done very little work with tin coatings, but we have been impressed by the smooth appearance of the metal-coated fiber surface and the fact that some of our best strength results (in excess of 900,000 psi) have been achieved with tin-coated fibers.

6. Optical Properties Characterization

a. Spectral Insertion Loss

There are currently two techniques[1] for measuring total attenuation in multimode fibers. The most widely used technique is to measure the optical power transmitted through two lengths of a fiber with input and output coupling losses held constant.[2] The second technique, discussed later, employs an optical time-domain reflectometer (OTDR).

---

[1] E.A.J. Marcatili, "Factors Affecting Practical Attenuation and Dispersion Measurements," digest of technical papers presented at Topical Meeting on Optical Fiber Transmission II, February 22-24, 1977, Williamsburg, Virginia.

[2] D.B. Keck and A.R. Tynes, "Spectral Response of Low Loss Optical Waveguides," Appl. Optics 11, 1502 (1972).

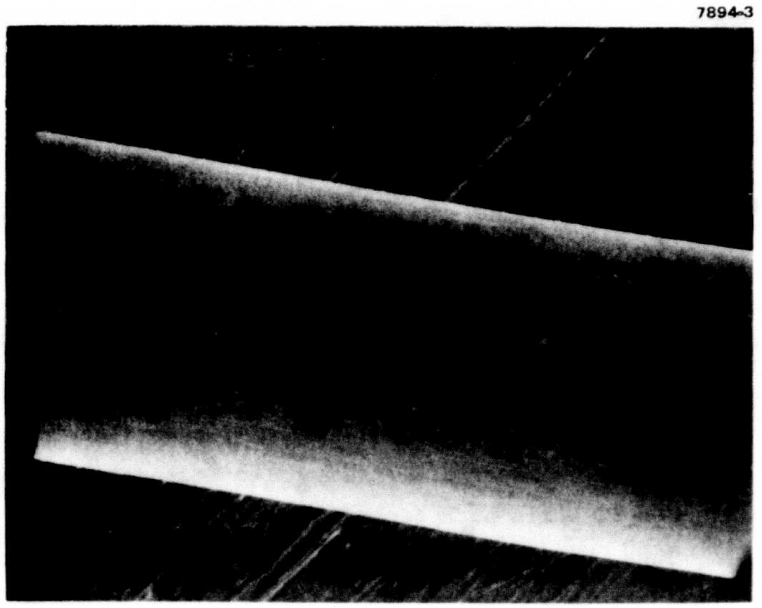

(a) Unstrained surface

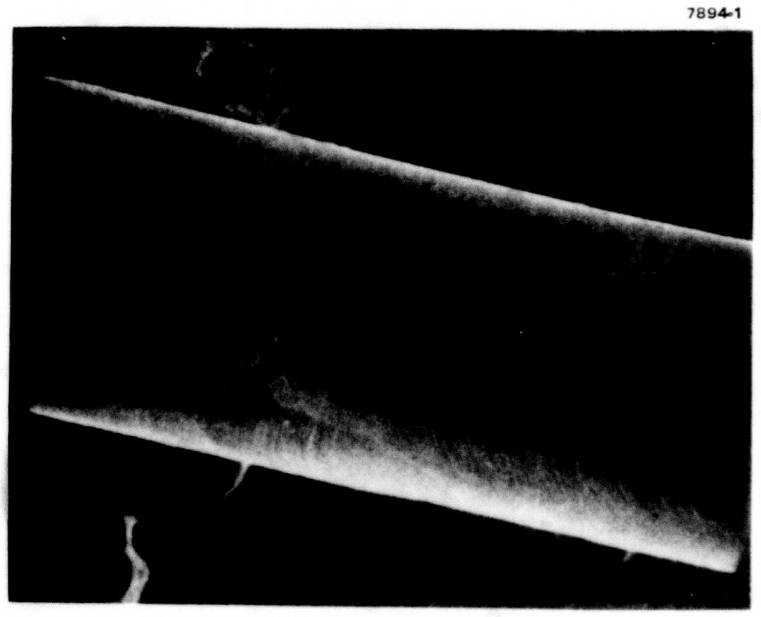

(b) After 20 cycles

Figure 16. The effects of cyclic straining on the aluminum jacket. The progressive development of slip planes is pronounced.

(c) After 250 cycles

Figure 16. Continued.

Table 3. Recrystallization Temperatures

Metal	Approximate Lowest Recrystallization Temperature, °F
Iron	840
Nickel	1110
Gold	390
Silver	390[a]
Copper	390
Aluminum	300
Platinum	840
Magnesium	300
Tantalum	1830
Tungsten	2190
Molybdenum	1650
Zinc	Room temperature
Lead	Below room temperature
Tin	Below room temperature
Cadmium	About room temperature

[a]Indications are that, under certain conditions, silver will recrystallize at lower temperatures.

6376

The optical power at a propagation distance X in the fiber waveguide can be expressed as

$$P(X) = P(X_1) \exp\left[- \int_{X_1}^{X} \alpha(x)dx \right] , \qquad (1)$$

where $\alpha(x)$ is the loss coefficient (which, in general, is dependent on both position and launch conditions) and $P(X_1)$ is the power in the fiber at position X_1. If the loss coefficient is constant, the above expression reduces to Beer's law. The attenuation coefficient measured by insertion loss is therefore an average given by

$$\bar{\alpha}(X_1, X_2) = \frac{1}{X_2 - X_1} \int_{X_1}^{X_2} \alpha(x)dx , \qquad (2)$$

where X_1 and X_2 are the two fiber lengths used in the measurement. This average may or may not equal the constant steady-state attenuation of the fiber. Individual modes propagating in a fiber have different losses. High-order modes, with higher penetration in the generally lossier cladding and more coupling to unguided modes via guide imperfections, have more loss than lower-order modes. This differential loss tends to be statistically compensated along the fiber by modal coupling. In fact, when complete compensation is achieved, a steady-state mode distribution is established which propagates with a characteristic attenuation constant.

In making insertion-loss attenuation measurements, it can be experimentally determined[1] whether or not the steady-state condition has been achieved. This can be done by measuring the far-field

[1] S. Zernon and D. Fellows, "Characterization of the Approach to Steady State and the Steady-State Properties of Multimode Optical Fibers Using LED Excitation," Optics Comm. 13, 198 (1975).

half-radiation angles θ_2 and θ_1 at fiber lengths X_2 and X_1, respectively. If $\theta_2 = \theta_1$, then each mode is propagating with the same attenuation and $\alpha(x)$ in Eq. 1 and 2 is constant. In that case, it would be valid to quote attenuation in dB/km. If $\theta_1 \neq \theta_2$, then the attenuation coefficient measured is the average attenuation for that particular length of fiber and for those coupling conditions. If X_1 is a very short length of fiber, then θ_1 can be taken to be the angular extent of the input beam (i.e., the launch numerical aperture).

A modern, versatile, phase-locked system has been constructed and used at HRL for determining the insertion loss of long lengths of communication-quality optical fiber. A schematic of the apparatus is shown in Figure 17. A white-light source is imaged on the entrance slit by lens L_1. This beam is chopped mechanically, and a reference signal is generated for the lock-in amplifier. The monochromator selects the light frequency of interest and presents that frequency at the output slit. Several exit slits are available for simulating narrow bandwidth sources such as lasers or broadband sources such as LEDs. Lens L_2 collimates the light from the monochromator. Aperture stops are placed in the beam to vary the launch numerical aperture. The maximum currently available numerical aperture is 0.35, set by the microscope objective, lens L_3. The trumpet tube shown next to it holds the fiber in position and is adjustable in all three dimensions. The output of the fiber is monitored by a photomultiplier coupled to the lock-in amplifier. The entire apparatus is supported on a precision floating optical table to isolate it from the surrounding environment. Measurements can also be made using coherent sources. Coherent measurements require that a simple folding mirror be placed in the system to couple in the coherent source.

b. Optical Time Domain Reflectometry

The loss measurement techniques discussed above provide the insertion loss for a given fiber length, but give no information concerning the length dependence of the loss. If the loss varies with length, then quoting attenuation as determined by insertion-loss measurements in dB/km may not be an adequate characterization of the fiber.

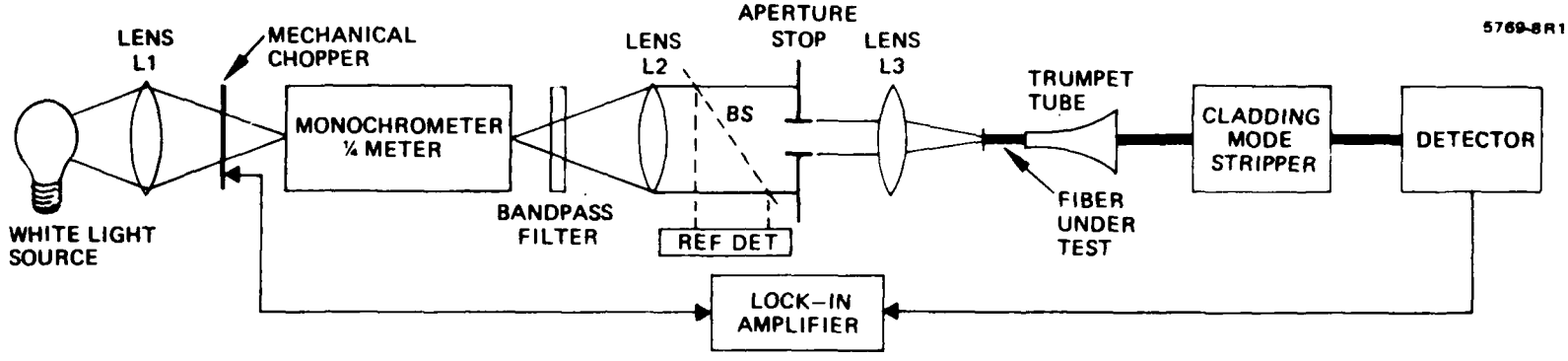

Figure 17. Schematic of HRL fiber insertion loss measurement apparatus. Spectral measurements over the range from about 0.6 to 1.0 μm are routinely made with this laboratory system.

A new measurement technique utilizing an OTDR, recently reported,[1-6] allows the length-dependence of the fiber attenuation to be displayed. This technique, based on the analysis of backscattered light in the fiber, requires neither cutting the fiber nor access to both ends of the fiber. Instead, a pulse of light is launched into the fiber in the forward direction as illustrated in Figure 18. The waveform of the return light pulse is detected by a photodetector and processed with a boxcar integrator. The return waveform consists of three distinct segments: (1) an initial pulse, which results from any nondirectionality in the input coupling mechanism; (2) a long tail caused by the distributed Rayleigh scattering that occurs as the input pulse propagates down the fiber; and (3) pulses caused by the discrete reflections that may occur along the fiber length as a result of fiber imperfections, in-line connectors, or the Fresnel reflection incurred from the end of the fiber. The Rayleigh-scattered return can be used to extract the attenuation coefficient. The time dependence of the detected backscattered power can be converted to a length dependence by multiplying by the velocity of light in the fiber core. The detected backscatter power may be expressed as

$$P(X) = k\, P(o) e^{-2\bar{\alpha}(X)X} \quad , \tag{3}$$

---

[1] M.K. Barnoski and S.M. Jensen, "Fiber Waveguides: A Novel Technique for Investigating Attenuation Characteristics," Appl. Opt. 15, 2112 (1976).

[2] M.K. Barnoski, M.D. Rourke, and S.M. Jensen, Proc. 2nd European Conference on Fiber Communication, September 27-30, 1976, Paris, France.

[3] S.D. Personick, "Photon Probe – An Optical-Fiber Time Domain Reflectometer," BSTF 56, 355 (1977).

[4] S.D. Personick, "New Results on Optical Time Domain Reflectometry," Technical Digest 1977 International Conference on Integrated Optics and Optical Fiber Communication, July 1977, Tokyo, Japan.

[5] M.K. Barnoski, M.D. Rourke, S.M. Jensen, and R.T. Melville, "An Optical Time Domain Reflectometer," Appl. Opt. 16, 2375 (1977).

[6] B. Costa and B. Sordo, "Experimental Study of Optical Fibers Attenuation by Modified Backscattering Technique," presented at 3rd European Conference on Fiber Communication, September 1977, Munich, Germany.

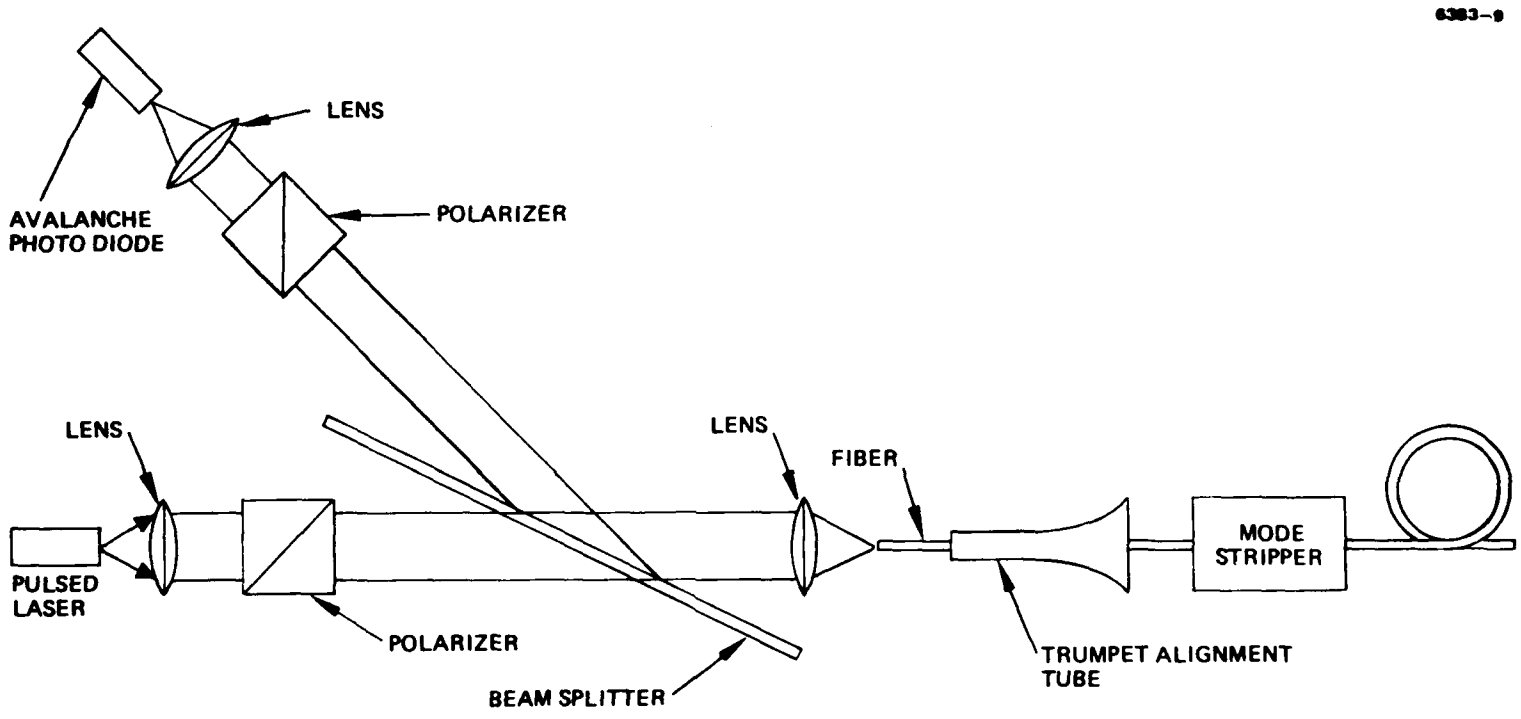

Figure 18. OTDR directional coupler employing a beam splitter and cross polarizers. The OTDR technique provides a spatially resolved measure of the total attenuation along the fiber waveguide without the need for cutting the fiber into shorter pieces. The spatial resolution is determined by the width of the input light pulse.

where X is a position along the fiber length, k is a constant, P(o) is the power launched into the fiber at the input, and $\alpha(X)$ is the average total attenuation coefficient of the forward and backscattered signals. The constant k is proportional to the square of the numerical aperture and the attenuation coefficient due to scattering. In general, k also may be dependent on position X.

Experimental results reported in the literature[1-5] have clearly demonstrated that this backscattering technique can be used to determine fiber attenuation characteristics. The method offers the advantages of requiring access to only one end of the fiber and of not requiring that the fiber be cut. In addition, by inspecting the return waveform, it is possible to determine if the attenuation of the fiber is actually constant over its length.

c. Experimental Results Obtained on Metal-Jacketed Waveguides

Total attenuation of uncoated and metal-coated step-index fibers manufactured at Hughes has been measured by the insertion-loss technique and with the OTDR. The range of observed attenuation is quite large, covering a span from 4 dB/km for the best section of Sn-coated waveguides to over 100 dB/km for fibers drawn from early preforms of questionable quality. In the more recently prepared waveguides, the attenuation was found by optical time domain reflectometry to vary along the length of the waveguide and generally to lie in the range from about 5 to 30 dB/km. In several instances, we have been able to correlate

---

[1] M.K. Barnoski and S.M. Jensen, "Fiber Waveguides: A Novel Technique for Investigating Attenuation Characteristics," Appl. Opt. 15, 2112 (1976).

[2] M.K. Barnoski, M.D. Rourke, and S.M. Jensen, Proc. 2nd European Conference on Fiber Communication, September 27-30, 1976, Paris, France.

[3] S.D. Personick, "Photon Probe — An Optical-Fiber Time Domain Reflectometer," BSTF 56, 355 (1977).

[4] S.D. Personick, "New Results on Optical Time Domain Reflectometry," Technical Digest 1977 International Conference on Integrated Optics and Optical Fiber Communication, July 1977, Tokyo, Japan.

[5] M.K. Barnoski, M.D. Rourke, S.M. Jensen, and R.T. Melville, "An Optical Time Domain Reflectometer," Appl. Opt. 16, 2375 (1977).

discrete insertion losses in the uncoated waveguide with visible scattering centers, thought to be small bubbles or other perturbations in the core-clad interface. We attribute these mainly to defects incorporated into the CVD preform during its manufacture.

We are also attempting to find meaningful correlations between the measured attenuation and other known characteristics of the metal-coated waveguide. In particular, the data strongly suggest that the metal coating in some way causes microbending of the waveguide. Previous studies by Miller[1] on plastic-coated waveguides incorporated into ribbon cables confirmed the importance of controllable waveguide parameters such as NA, the ratio of cladding thickness to core diameter, and overall fiber diameter in determining the magnitude of excess attenuation caused by microbending. We have applied these same parametric analyses to our data on metal-coated waveguide with limited success. We suspect that additional parameters (for example, see the discussion in Section 1.A.1 on periodic hillocks) are important in addition to the geometric factors listed above. As we gain better control of both the metal application and the preform fabrication processes, we would expect these added effects to diminish to the point where the systematic variations due to the parameters identified by Miller dominate the excess loss.

For example, the attenuation data show one consistent trend that supports the contention that the excess loss introduced by the metal jacket has a strong microbend component. In several recent experiments, we changed the diameter of the fiber during the draw to obtain two different-diameter metal-coated fibers from the same preform. In all cases, we find with OTDR measurements that the attenuation in the larger-diameter section is less than that in the smaller-diameter section. This consistent result strongly indicates that the extra rigidity of the larger-diameter fiber minimizes the extent of microbending induced by the metal jacket. Figure 19 shows the trace of an OTDR measurement

---

[1] C.M. Miller, BSTJ 55, 929-935 (1976).

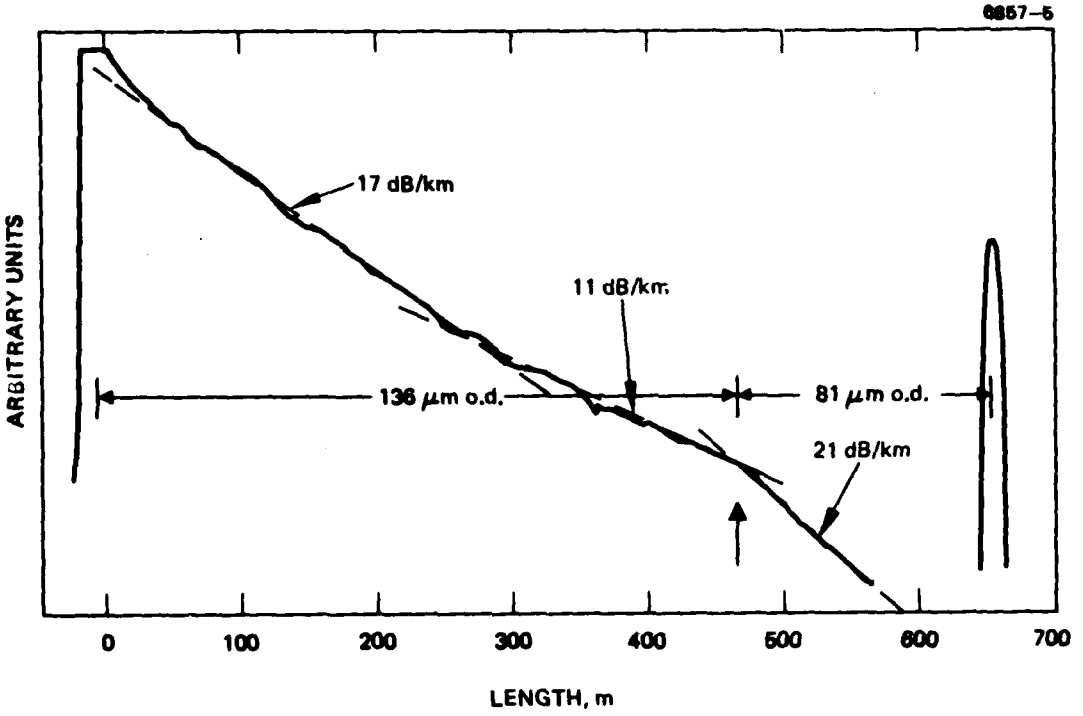

Figure 19. Attenuation measured by optical time domain reflectometry on a metal-coated step index waveguide. The large arrow points to the location of a diameter change in the fiber which results in a change in the attenuation. This effect has been observed whenever the fiber diameter undergoes a marked change.

on a metal-coated waveguide with two different diameters. The slope of the curve is an indication of the attenuation, and a distinct change in slope is quite evident when the fiber diameter changes.

At present, we do not have a complete understanding of all the contributors to the attenuation found in metal-jacketed step-index waveguides. It is apparent that the quality of both the metal coating and the preform is significant. When the preform is uniform, the loss is low (as in Figure 19). If the metal jacket is well behaved, then sections of fiber like those in Figure 3 are obtained. Several months ago we also obtained the data shown in Figure 20 from pieces of coated and uncoated waveguide drawn at different times from the same preform. The curve represents the attenuation measured by the spectral insertion-loss technique on a 250-m section of uncoated (bare glass) step-index waveguide. The discrete points indicate the loss measured at convenient laser wavelengths for this uncoated section and in a 60-m-long piece from the same preform, which had been coated with Al. These data suggest that the excess loss attributable to the metal jacket can be as low as 5 dB/km. For Sn-clad waveguide, we have measured total attenuation below 5 dB/km, as shown in Figure 21.

More recently, we have examined many metal-clad waveguides and have found a useful correlation between the excess loss caused by the presence of the metal jacket and a factor incorporating the waveguide parameters mentioned earlier. This factor, designated F, was found empirically to give the best fit to both our metal-clad fiber results and to those of Miller[1] for ribbon cable when the square root of the ratio of clad thickness to diameter and the first power of the refractive index difference were employed:

$$F = (t/d)^{1/2} \cdot \Delta n \quad .$$

[1] C.M. Miller, BSTJ 55, 929-935 (1976).

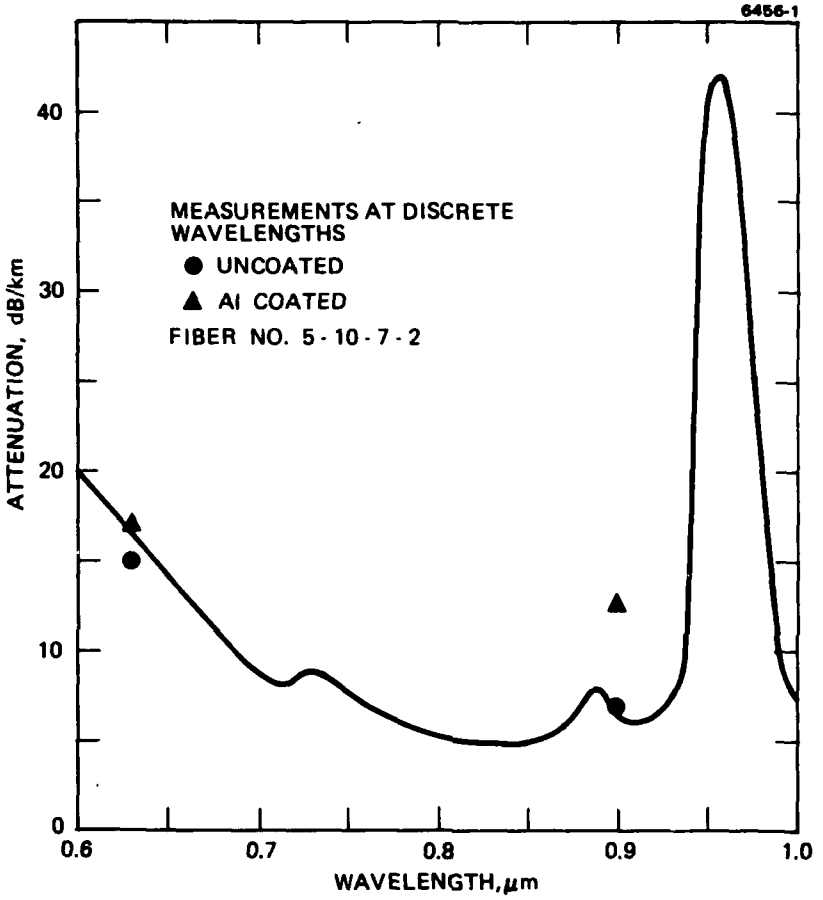

Figure 20. Optical attenuation of an experimental waveguide. The solid curve was obtained from a 250-m length of bare waveguide. The points were obtained at laser wavelengths on a 50-m section of Al-coated fiber drawn from the same preform.

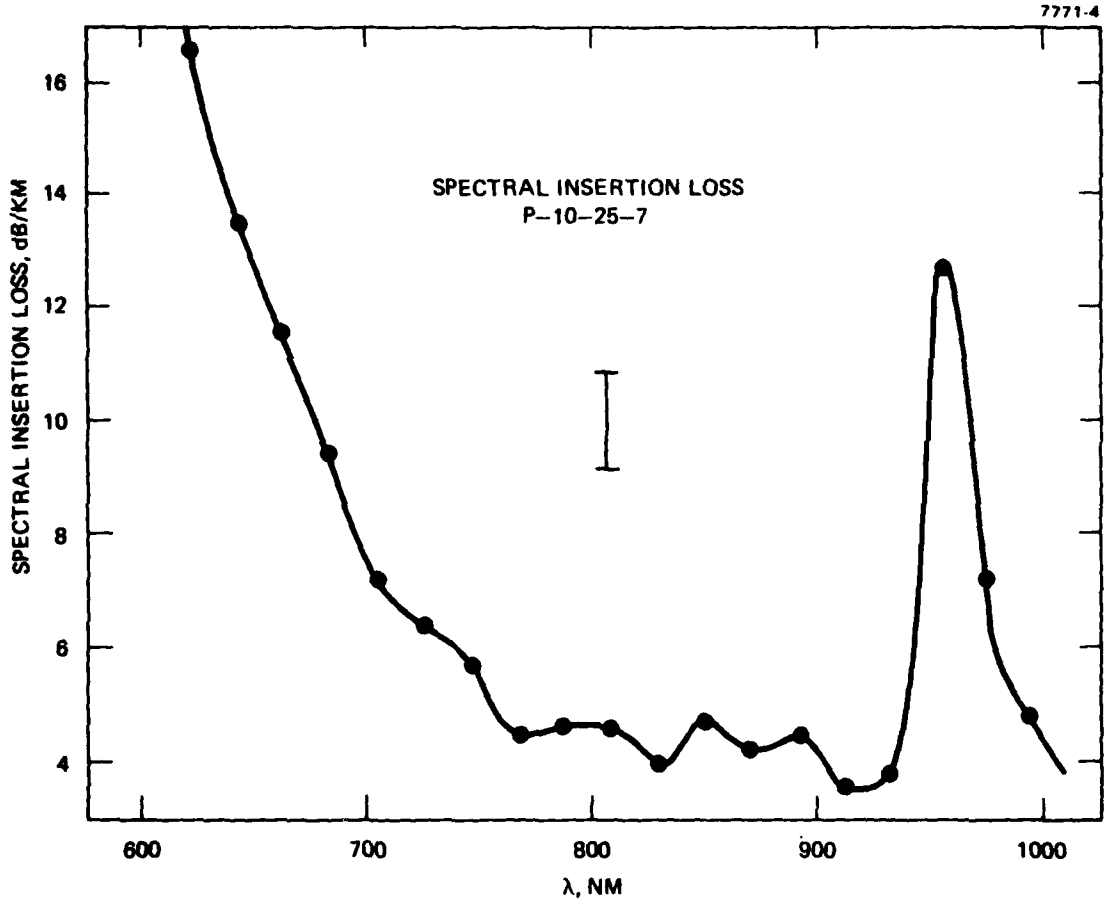

Figure 21. Spectral insertion loss of a Sn-coated fiber. The total attenuation at 920 nm of <4 dB/km is the lowest yet measured for a metal-jacketed waveguide.

When both sets of data were plotted against this parameter, the groupings shown in Figure 22 were obtained. Functional relationships of the form

$$L = A\ F^{B}$$

for the excess loss L are indicated by the straight lines for each set of data. Correlation coefficients (r^2) for both curves are about 0.85, indicating a sufficiently good correlation to be useful in future design tradeoff studies. As we collect additional data, we expect to find expressions with even higher correlation coefficients.

d. Strain-Induced Attenuation

In a previous program (heavily complemented with IR&D funds), measurements were initiated to determine the effect of axial strain on the optical attenuation in waveguides coated with both metal and plastic. The data showed that applying tension to each of the waveguide specimens caused an excess loss; however, more measurements will be required to identify clearly the source of this loss. The short length of the available test corridor limited this exploratory work to samples up to 70 m in length. Although we are confident in the absolute values of the change in excess attenuation measured for these relatively short fiber lengths, the validity of extrapolating this insertion loss to a long-length value (dB/km) has not yet been established. For example, the observed excess loss could possibly be due to termination effects where the fibers interact with the end pulleys (in the experimental arrangement described below) rather than a loss which increases monotonically with fiber length between the pulleys. Additional testing on longer fiber spans is contemplated in future work.

The experimental setup used in these experiments is shown in Figure 23. One end of the fiber under test is wrapped several times around a 10-cm spool (spool "A" in Figure 23) and is taped in place on the spool to ensure that the fiber does not slip. Next, the fiber is laid out down a 70-m-long hall. During layout, care is taken to prevent the fiber from rotating, thus ensuring that the fiber is subjected to

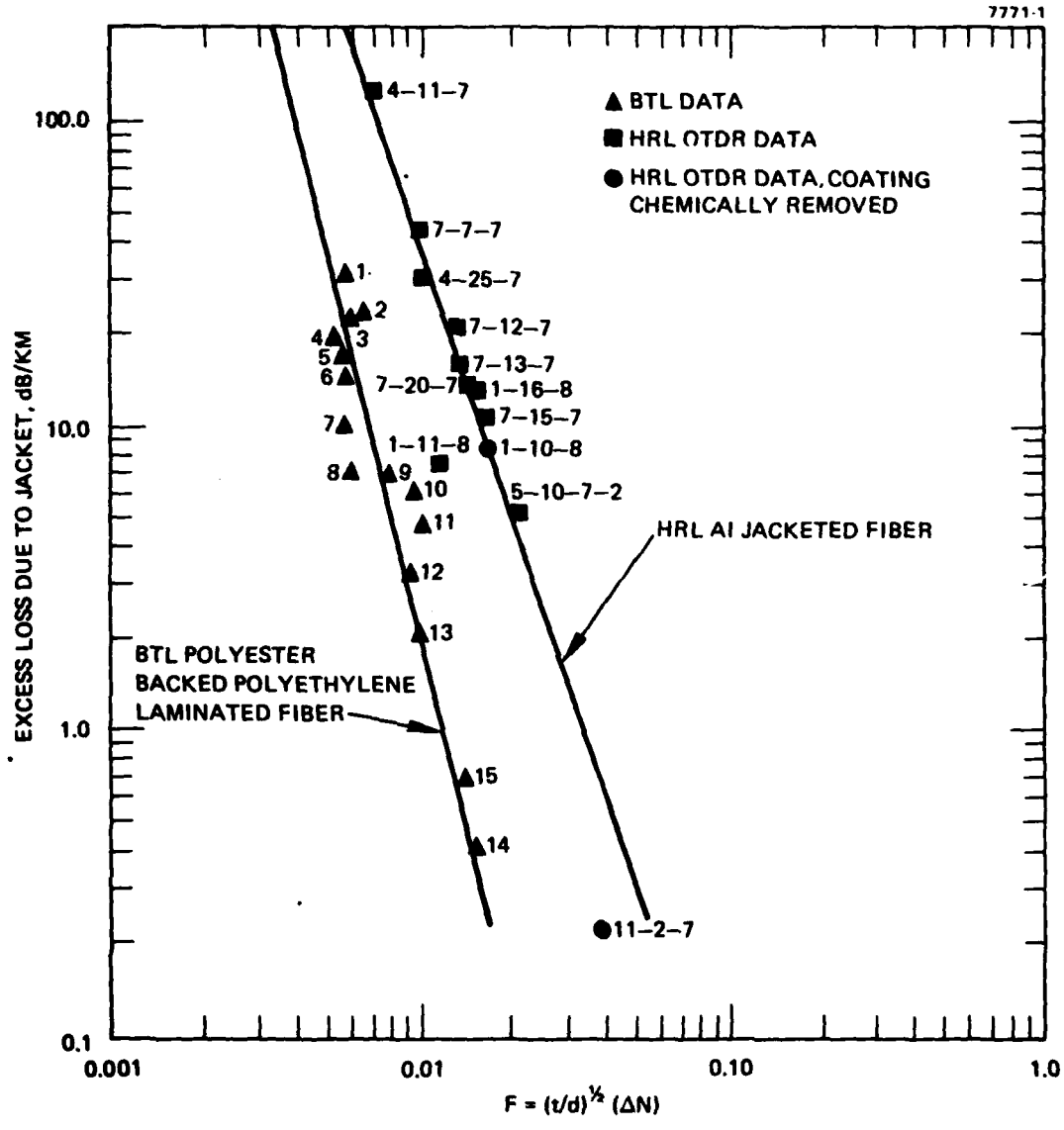

Figure 22. Excess loss in plastic-clad and metal-clad waveguide. The empirically determined factor F provides a useful relationship for waveguide design.

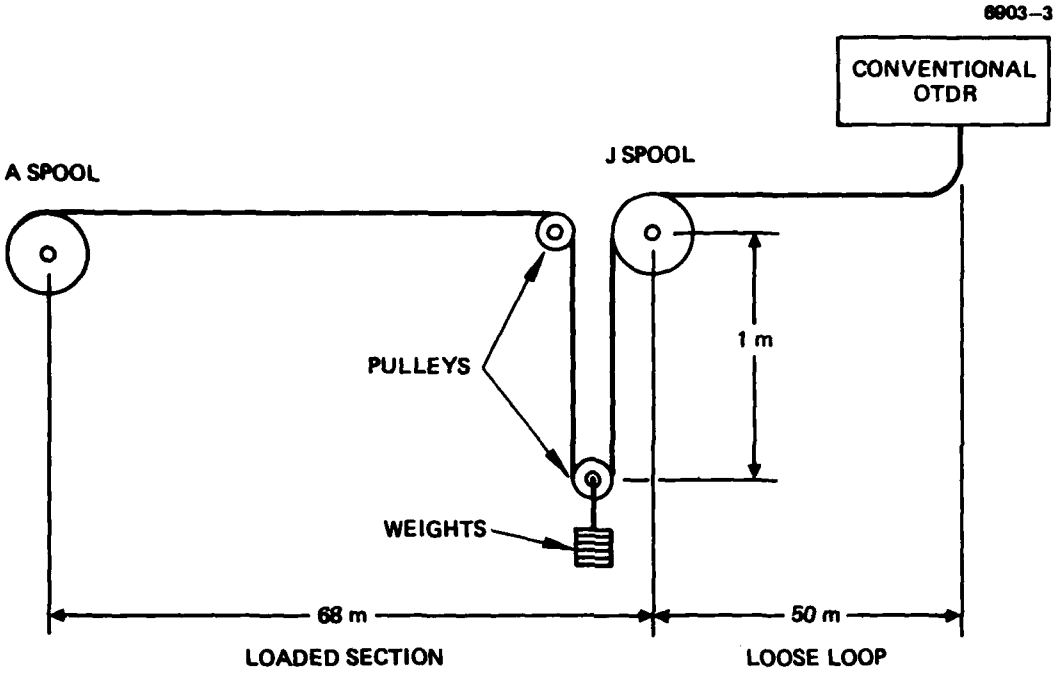

Figure 23. Experimental setup for strain-induced optical attenuation measurements. The axial strain is controlled by the applied mass and is measured by the change in height of the pendant pulley.

longitudinal strain only. Ten small hooks placed at approximately equal intervals down the length of the hall support the fiber. At the end of the hall, a 5-cm o.d. pulley bends the fiber 90°. Approximately 1 m after the first pulley, a second 5-cm o.d. pulley bends the fiber 180°, forming a loop of fiber. Mass is attached to this second pulley to provide a controlled axial stress in the fiber. A second 10-cm spool (spool J in Figure 23) is used to secure the fiber at this end of the hall. Several loops of fiber are wrapped around spool J and are taped in place, again ensuring that the fiber will not slip. The remaining fiber is routed back to the optical characterization laboratory and placed into the standard OTDR setup. Since this last piece of fiber is never loaded, it shows no deviation from its initial loss.

When pulley A and the platform for holding the applied mass (total platform mass 110 gm) were placed on the fiber, the position of the bottom of the platform was marked, and an OTDR characterization of the fiber was obtained. This condition is referred to as the unloaded condition. These initial position and OTDR-characterization data points were recorded as reference points from which deviation would be measured on subsequent loading. Mass was then added to pulley A in 50-gm increments and platform position and loss data points were obtained for each mass.

The excess loss measurement which was made was an insertion loss measurement even though it was performed with the OTDR apparatus of Figure 18. The data were obtained by performing a complete OTDR characterization of the fiber in the unloaded condition. The amplitude of the signal, which was backscattered just prior to the Fresnel reflection from the distant ends of the fiber, was recorded as the value A_{ref}. The amplitude of the signal A_i, which was backscattered just prior to the Fresnel reflection, was recorded as each incremental mass was added to the weight platform. The change in A_i measured with respect to A_{ref} is the excess loss L and is calculated using the formula:

$$L = 10 \log \frac{A_i}{A_{ref}} \quad .$$

Several experimental data runs were performed on the Al-jacketed fiber P-8-11-7. Figure 24 is the strain versus applied-force curve obtained for this fiber. The data show two regions of distinctly different slope as force is being applied. This behavior, also observed in the Instron measurements, can be explained qualitatively. If a force of less than 2 Newtons (N) is placed on the structure, the Al and the waveguide will both be elastically elongated (the Young's moduli of SiO_2 and Al are nearly identical) and will share the load approximately in the ratio of their cross-sectional areas. If more force is applied, the Al coating will be plastically deformed and will support a varying but monotonically decreasing fraction of the load. The change in the load supported by the Al coating in this region is very small. Consequently, we assume in what follows that the coating, when it is plastically deformed, supports a fixed load. The remaining portion of the load is taken up by the waveguide, which continues to behave as an elastic body. Hysteresis, characteristic of cyclic plastic strain, is observed in both the loading and unloading cycles. A permanent elongation is apparent when the fiber is finally unloaded, indicating that the waveguide is under a longitudinal tension and the Al coating is under a longitudinal compression at the end of the initial loading cycle.

The second and all subsequent loading cycles begin at this permanently induced strain level and exhibit a single, lower slope until the Al again goes into plastic deformation. The second loading cycle exactly parallels the first cycle from this point on. The third and all subsequent cycles follow the second loading curve. The slope transitions occur at about 0.12% strain on loading and at 0.12% strain below the maximum strain on unloading.

The first time the fiber was stretched, the loss increased until the maximum stress had been applied (Figure 24). This loading portion of the curve exhibited an initial region of rapid, nearly linear increase of loss with strain. This behavior persisted until the Al coating reached its elastic limit (strain approximately 0.12%). Optical attenuation continued to increase but at a much reduced rate when the coating was strained beyond its elastic limit. This loss-change versus strain

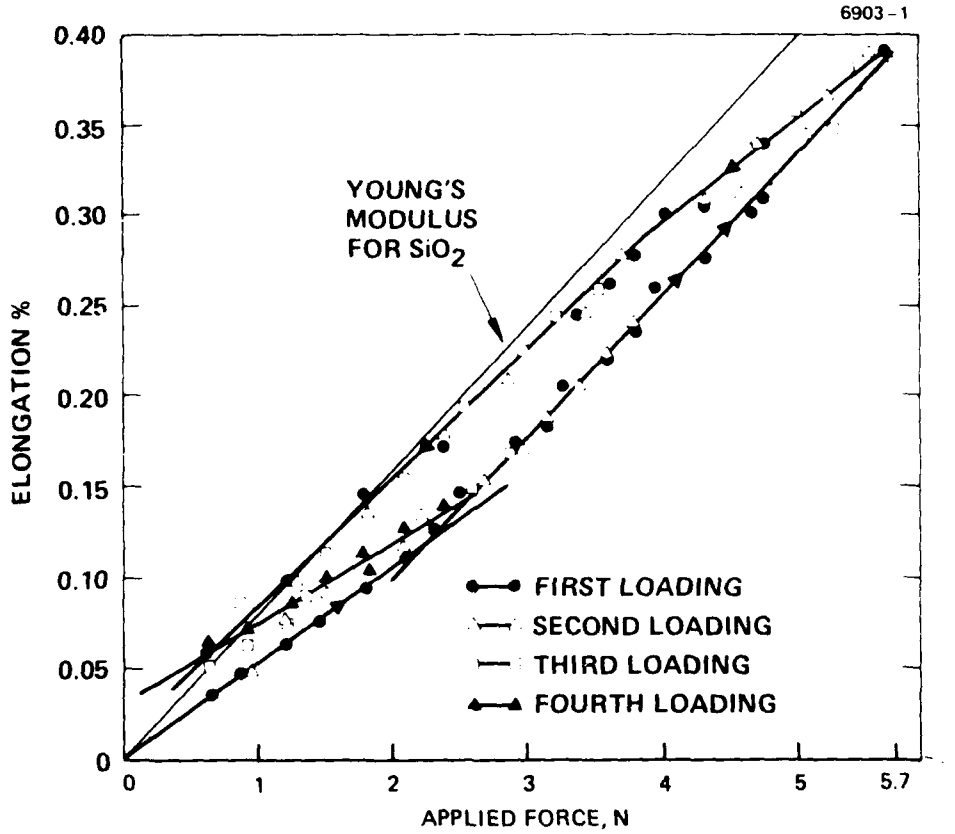

Figure 24. Strain-force relationship for an Al-clad waveguide. The hysteresis is caused by plastic deformation in the Al jacket.

behavior is similar to the behavior of the strain versus applied-force of Figure 23 and suggests some relationship between the coating mechanical properties and the observed excess loss.

The loss dropped dramatically to a value near the initial attenuation as the load was removed (unloading portion of Figure 25). This is conclusive evidence that the primary excess-loss mechanism is not strain-induced birefringence, since there is still considerable longitudinal strain remaining in the fiber at this point. The loss monotonically increased as the remaining load was removed. Again, there is an apparent correlation with the coating mechanical properties.

The loss initially decreased as force was applied during the second loading cycle (Figure 26). This behavior persisted until the 0.12% strain level was reached. The loss monotonically increased when the load was further increased, driving the Al into plastic deformation. The unloading curve parallels the first cycle unloading curve. This same behavior was exhibited on subsequent load cycling experiments performed on this fiber. Unfortunately, dc drift in the ODTR electronics precluded taking data beyond the third loading cycle.

Initial stretching experiments were also performed on 80 m of the tin-coated fiber P-10-25-7. Figure 27 shows the strain versus applied-force curve for this Sn-coated fiber. Notice that there is mechanical hysteresis in these data similar to that in the Al-coated sample data; however, the permanent elongation resulting after a single loading cycle is much smaller than it was in the case of the Al coating.

Because the fiber broke during the experiment, we did not obtain sufficient data to determine whether hysteresis exists in the optical-loss versus strain curve. Figure 28 shows the optical behavior of this fiber prior to its failure. The short length of the loaded fiber again precluded determining the absolute long-length attenuation in the fiber.

The measured elongation versus applied-force for a CGW EVA-coated fiber is shown in Figure 29. Notice that the loading and unloading curves exactly track. No permanent deformation of the fiber was measured. Also, the slope of the elongation versus load curve is substantially

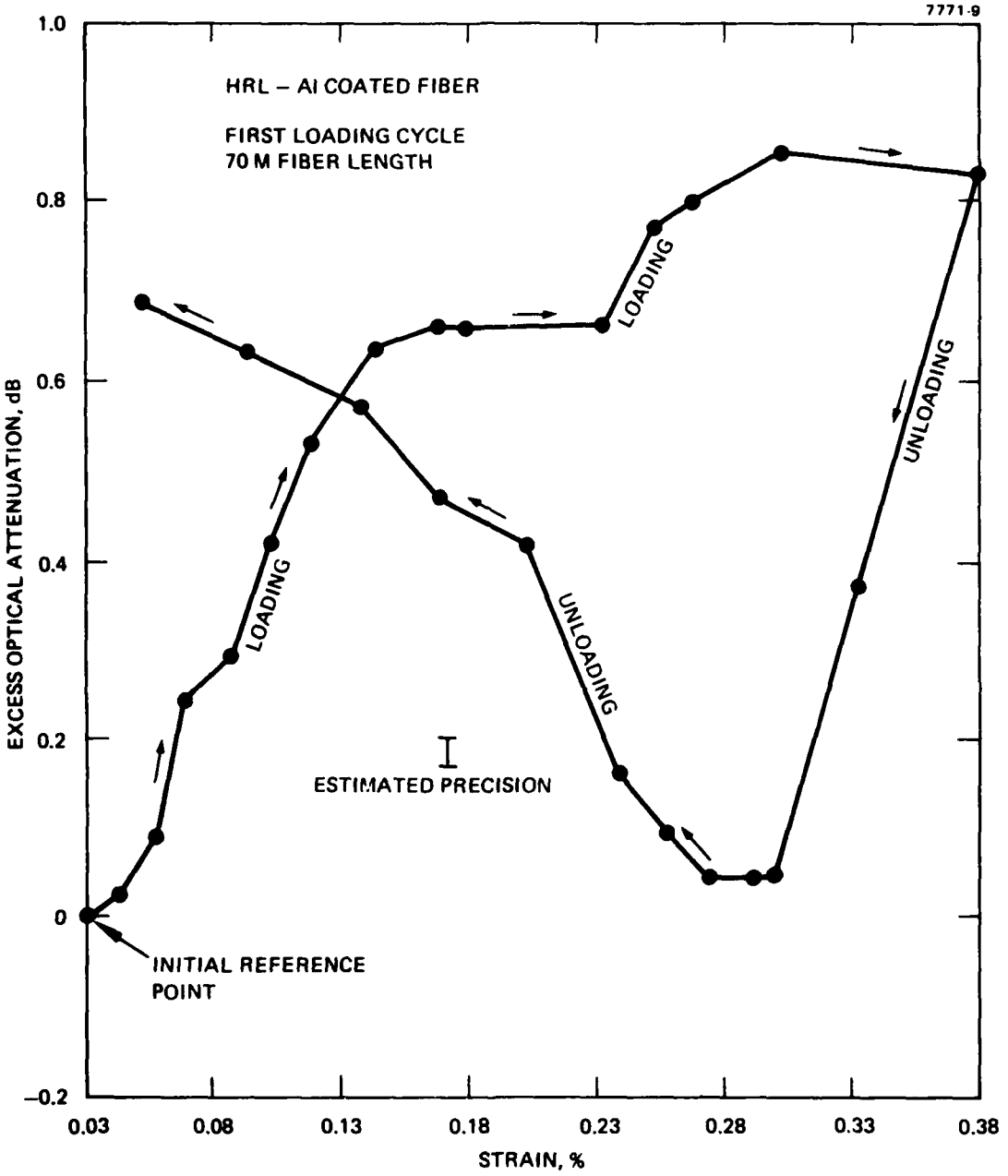

Figure 25. Excess loss exhibited by an Al-clad waveguide during the initial loading cycle. Some of the inflection points correspond roughly to the transitions from elastic to plastic response in the Al jacket.

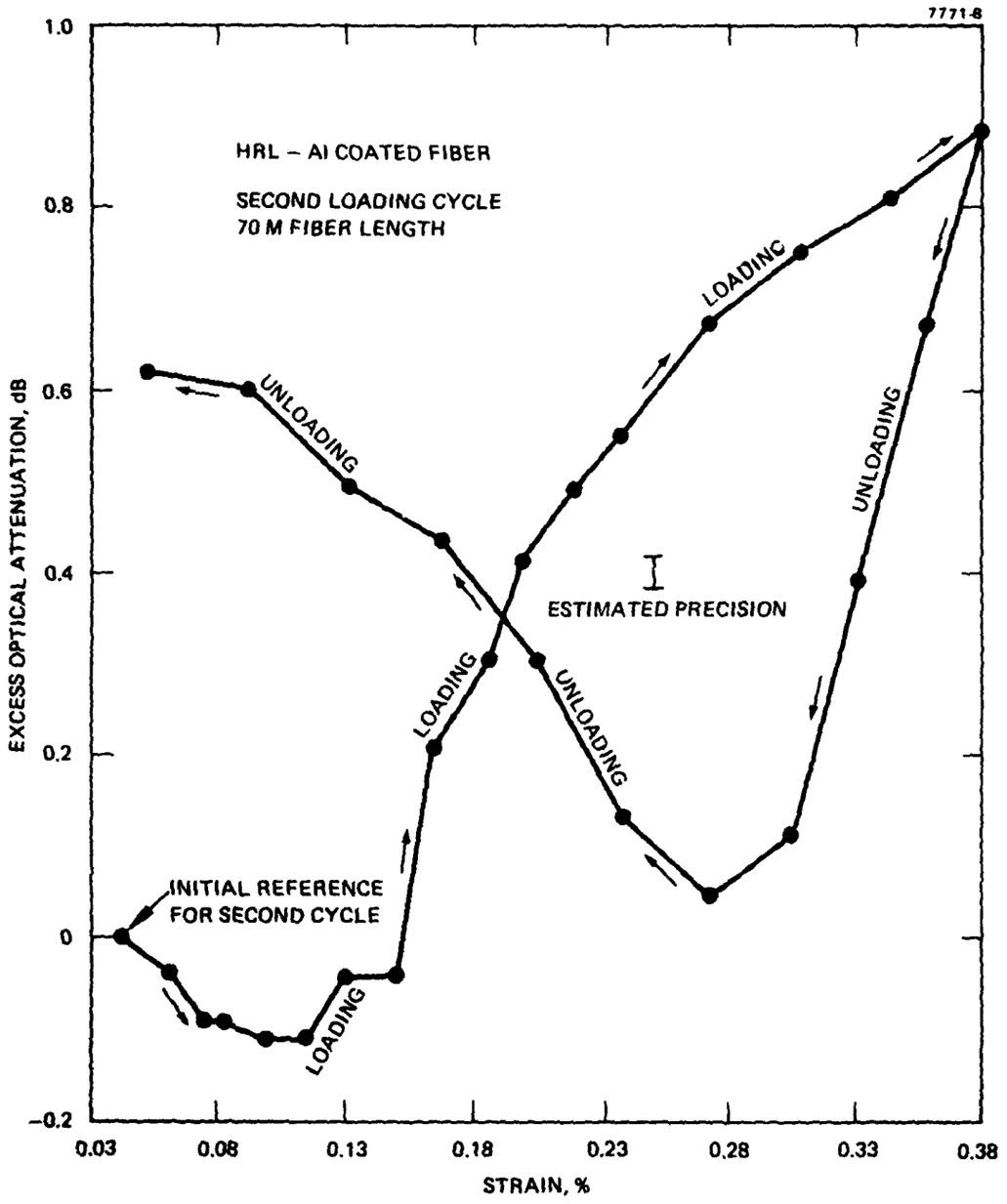

Figure 26. Excess loss during second loading cycle. For a waveguide already strained, there appears to be some relaxation in excess loss whenever the strain is reduced in the plastically deformed Al jacket.

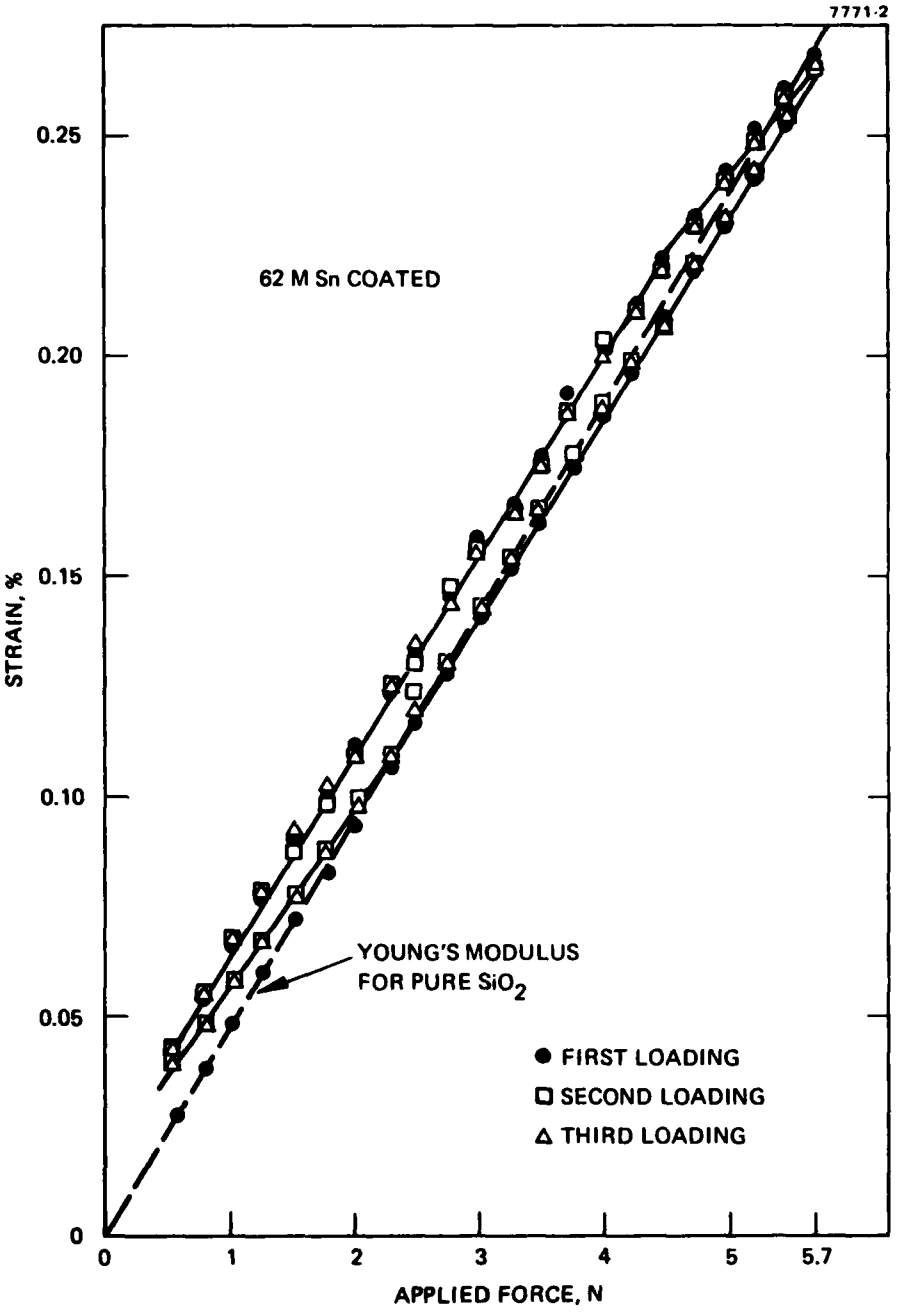

Figure 27. Axial strain in a Sn-coated waveguide. Because its diameter is 40% larger, this Sn-coated film shows less strain and hysteresis than the Al-clad waveguide.

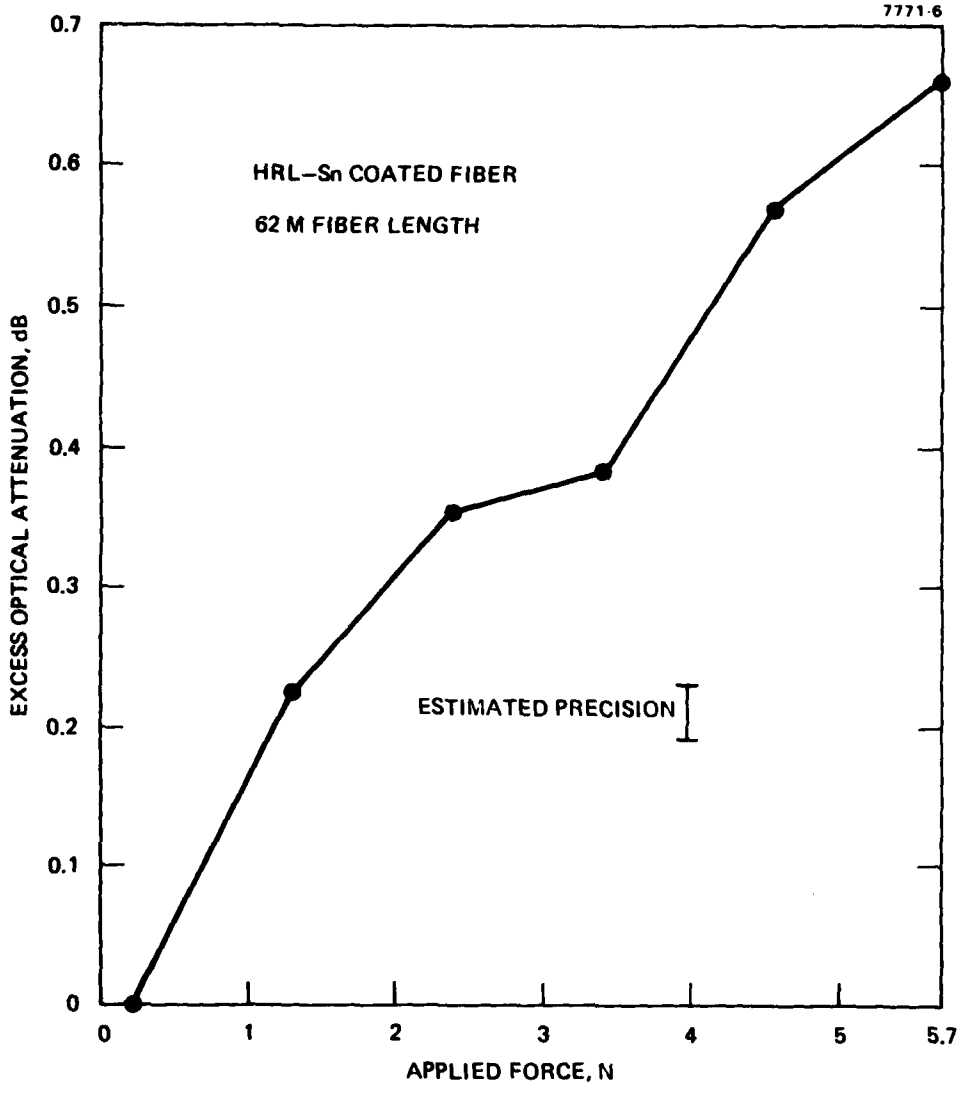

Figure 28. Excess loss for stretched Sn-clad step-index waveguide. These optical measurements were made after the stretching experiments of Figure 27. The lack of an initial dip in excess loss contrasts with the behavior of Al-clad waveguide and is probably a result of the relaxation possible in Sn because of its below-room-temperature recrystallization.

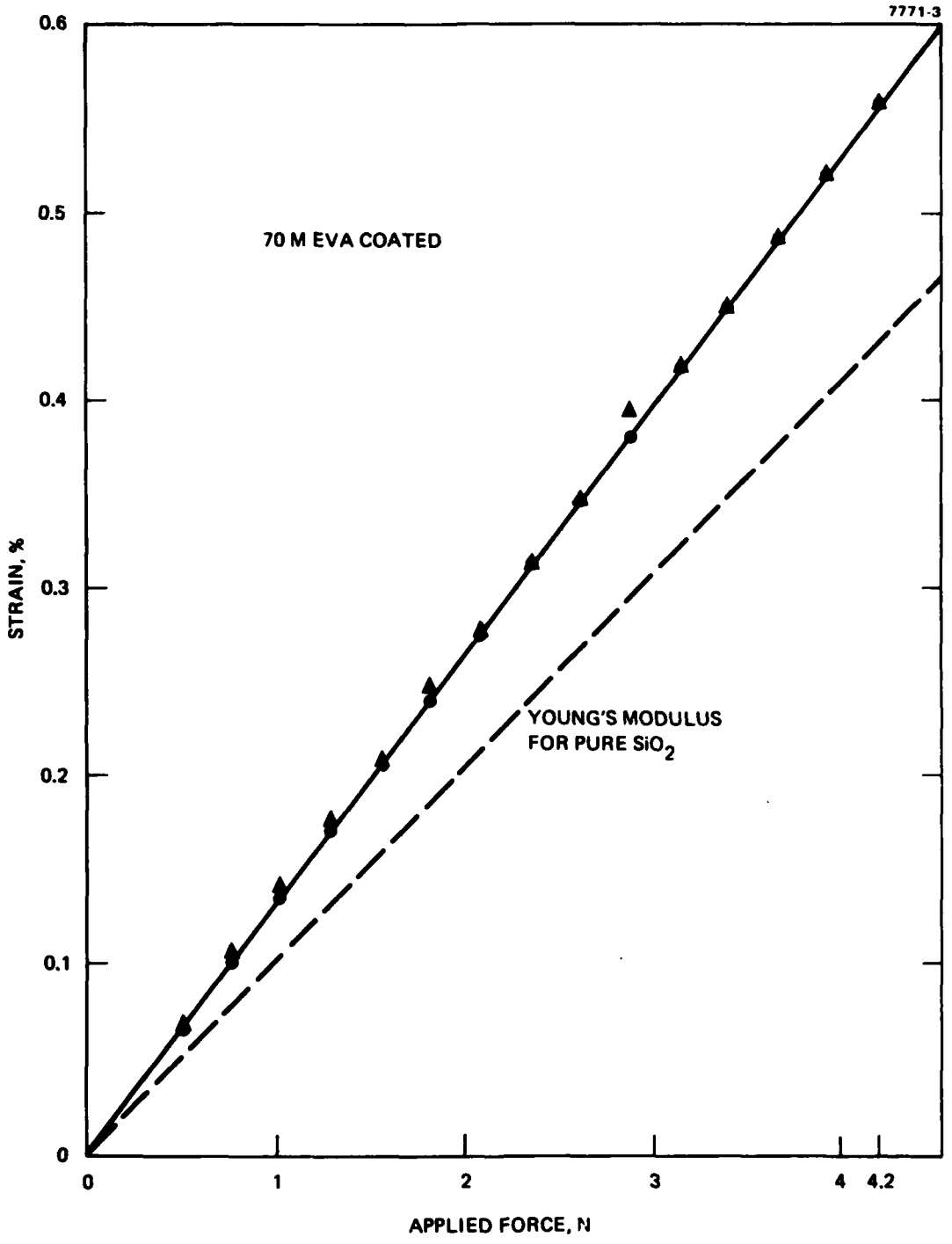

Figure 29. Axial strain in a plastic-coated waveguide. The EVA coating on this CGW waveguide does not show any plastic deformation. The departure from the elastic behavior of pure SiO_2 is caused by the large core of doped SiO_2 which has a lower Young's modulus.

greater than the Young's modulus for pure SiO_2. This result was expected since about 50% of the cross-sectional area of the CGW fiber is core glass. This large fraction of material is doped SiO_2 with a lower Young's modulus than pure SiO_2, and hence the mechanical behavior of the structure should be different from that of pure SiO_2. Both of the Hughes fibers, on the other hand, have core areas comprising approximately 10% of the fiber cross-sectional area. Hence, the effect of the core on mechanical behavior is expected to be small.

This CGW fiber was also broken during the first loading cycle of the optical measurement and consequently complete load cycling data are not available. Figure 30 shows the loss versus strain for this fiber as it was being loaded to the point where the fiber failed.

These initial experiments show that all measured waveguides, both plastic and metal coated, exhibited an increase in optical attenuation when subjected to strain. The Al and Sn coatings, but not the EVA plastic coating, also exhibited a mechanical hysteresis characteristic of cyclic plastic strain. Because of the radically different HRL and CGW fiber geometries and material composition, it is not possible to compare the relative effects of the coatings on optical properties. However, all three waveguides tested in the apparatus shown in Figure 23 exhibited an increase in the observed insertion loss as weights were added to increase the axial strain in the waveguide. Figure 31 shows these increases in attenuation as a function of the axial strain.

These stretching experiments are only the first attempt to explore optical effects induced by axial strain. To avoid possibly important termination effects, future experiments of this type will be conducted on much longer free lengths of fiber so that conventional OTDR measurements can be made on that portion of the waveguide remote from the terminations. Such experiments are planned in the near future.

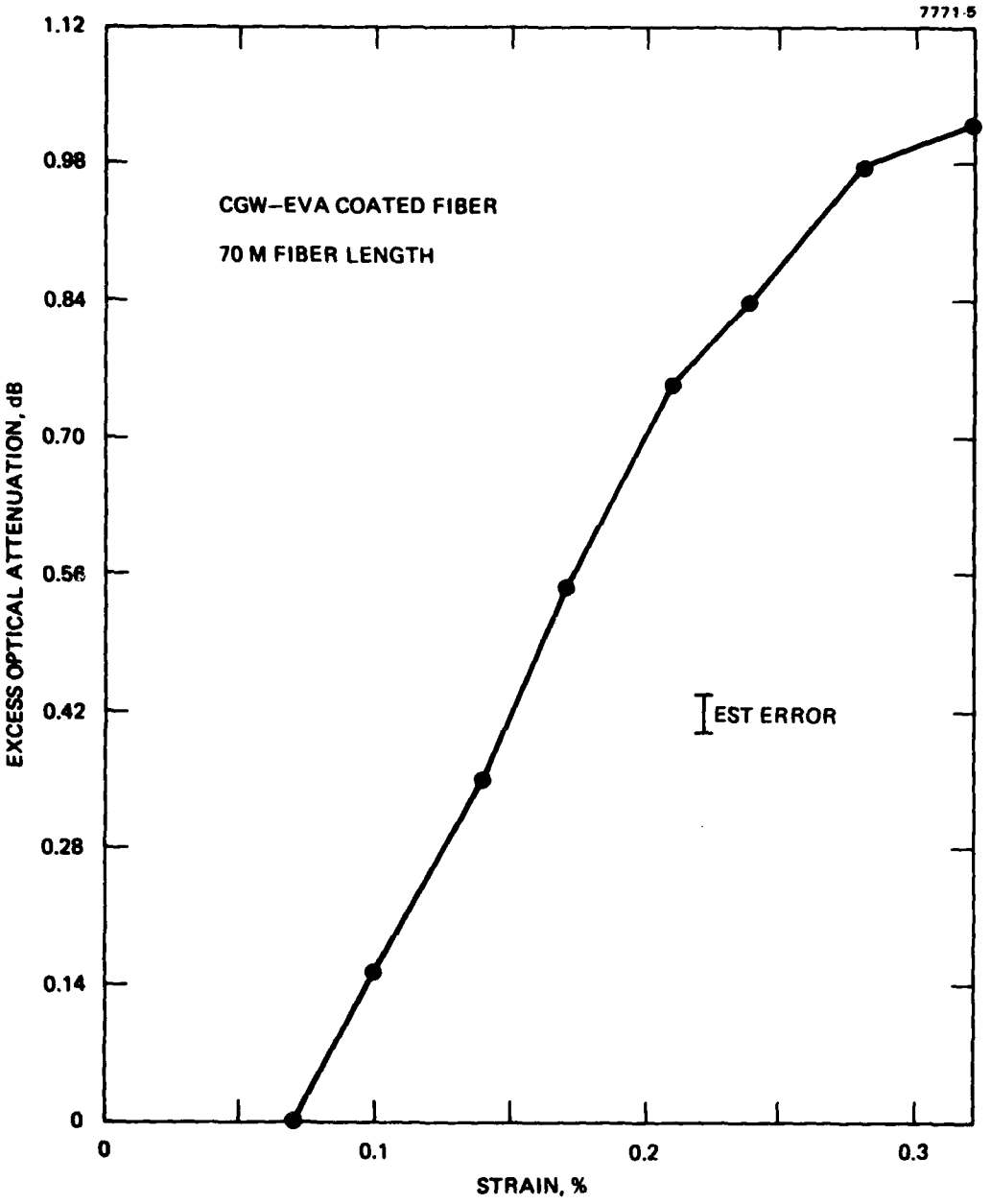

Figure 30. Observed excess optical attenuation exhibited by a CGW EVA coated fiber. The offset in strain is caused by the initial loading from the pulley before any weights are added.

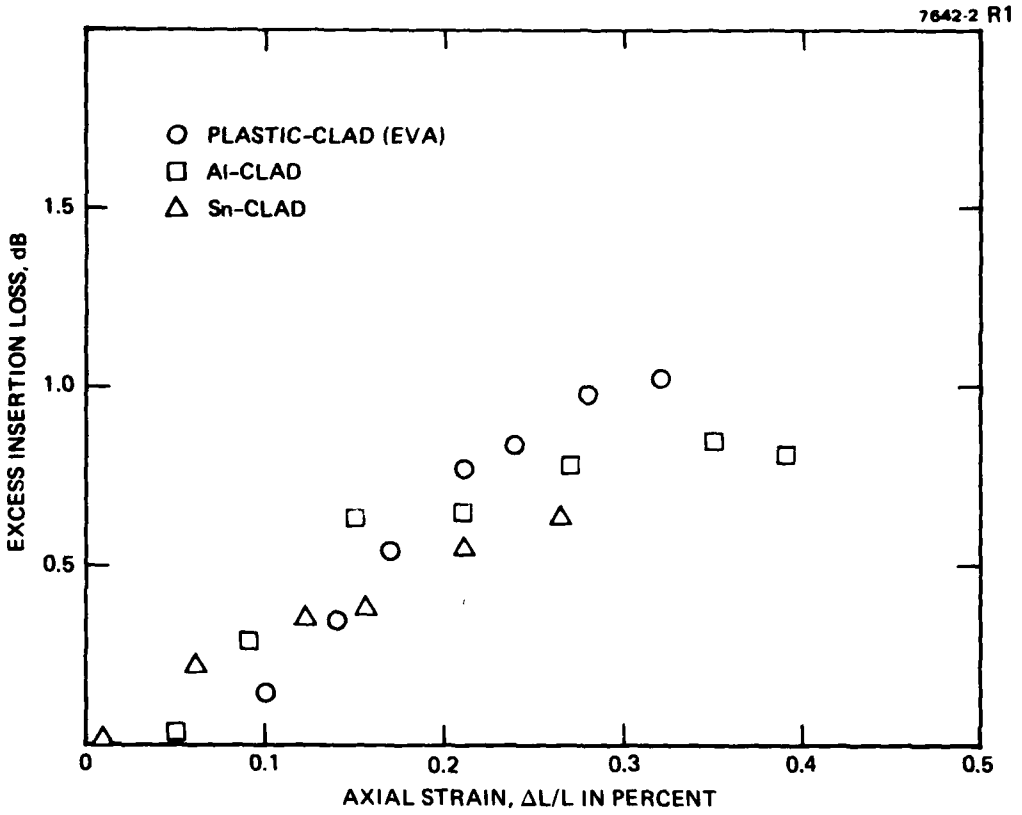

Figure 31. Excess loss observed in stretched waveguides. Because of possible end effects, the short sample lengths preclude extrapolation to long-length attenuation.

7. Cabling and Ruggedization

Although the metal-coated fiber is relatively strong and, for certain applications, self-supporting, the usual means of cable deployment and use require that the aluminum coat of the optical fiber be protected from rupture or scratching. Two approaches have recently been tried at HRL:

- Incorporation into a cable structure
- Ruggedization of individual fibers.

a. Cable Studies

The conventional approach toward protecting a delicate item is to enclose it in many layers of tougher material. Typically, a cable will consist of several essential elements such as:

- The fiber optical waveguides
- A coating (metal or plastic) immediately adjacent to the fiber to permit initial handling
- Load-carrying members such as steel or Kevlar fibers
- Fillers needed to preserve the form of the cable
- An outer abrasion-resistant sheath of neoprene, polyurethane, or other "tough" material.

Our present approach to cable structures incorporating many fiber-optical waveguides is to utilize the experience of the HAC Connecting Devices Division (CDD) in nearby Irvine, California, which has pioneered the design and development of flat cables for specialized purposes. This type of cable offers many advantages for use with fiber optics, especially the ease of making splices and connections in a multistrand cable. The machinery used at CDD for the production of flat cables containing fine wire is readily adaptable to the use of the metal-jacketed optical waveguide. Therefore, we have begun our cabling investigations by fabricating flat ribbon cables incorporating both four- and six-fiber waveguides into a flat polyimide (Kapton) ribbon. The polyimide film can readily be removed after it is softened by the heat from a soldering gun. This makes the individual metal-jacketed fibers readily accessible for incorporation into connectors or other termination devices.

One of the advantages of the six-strand flat cable configuration is that many layers of ribbon can be combined to make a cable bundle with a large number of individual waveguide channels. In Figure 32 a symmetrical 6 x 6 structure is shown constructed from flat ribbon cables. There is room in this cable structure for several electrical conductors, if desired, either as the additional elements seen in Figure 32 or as fine wires within the ribbons themselves. For larger capacity cables, this matrix concept can readily be extended to 10 x 10 or 12 x 12 arrays without greatly expanding the o.d. of the finished cable structure. This type of cable construction offers a more efficient use of the cable cross section than do the normal helical designs incorporating 6, 7, or 19 waveguides.

b. Ruggedization of Individual Fibers

There are occasions when the individual optical fiber should be enclosed in its own protective shell. Figure 33 shows one example of the type of ruggedizing being considered by HRL. This configuration is commercially available from Air Logistics Corporation (Pasadena, California), which prepared the sample contained in Figure 33. The aluminum-coated fiber is enclosed first in a soft silicone rubber for cushioning properties. The silicone-coated fiber is then encased in a fiberglass-polyester (or epoxy) composite. The fiberglass strands run parallel to the length of the cable and provide great axial load carrying capacity (200 lb for the sample in Figure 33). Such construction also lends substantial rigidity to the cable, although it can be easily spooled on 1-ft-diameter drums. Because the fiberglass-polyester shell has very high crushing strengths, the completed, ruggedized fiber can be stepped on, dragged over rocks and sharp edges, etc. without damage.

B. PROGRAM APPROACH

The goal of 10-km lengths of low-loss fiber-optical waveguides capable of surviving 2% strain for several years is a very ambitious one. We are convinced that there are no shortcuts that will result in instant success in achieving these goals. Rather, we foresee a considerable amount

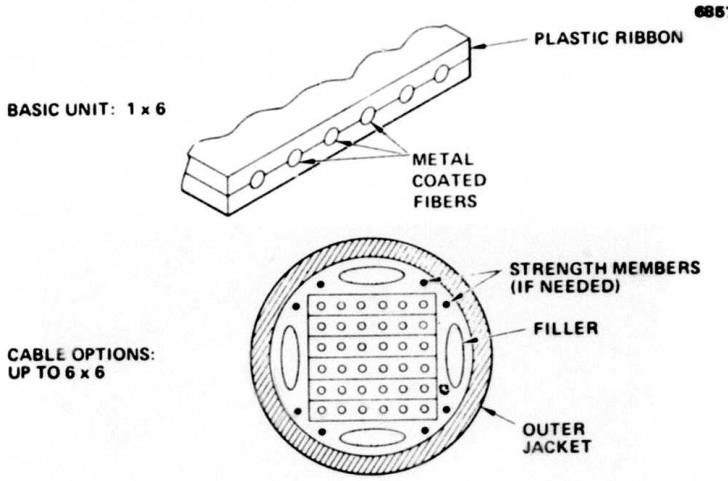

(a) Cross section

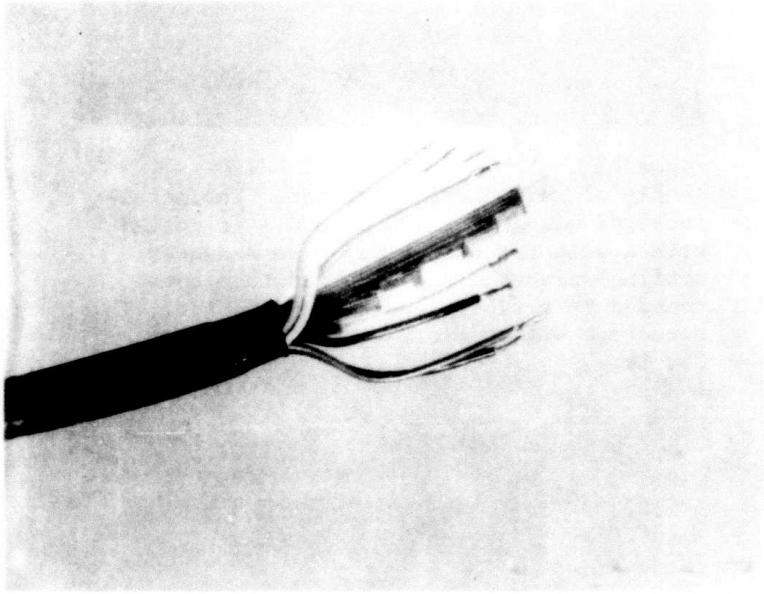

(b) Actual section of cable stripped to show the six ribbons.

Figure 32. Circular cable containing six plastic ribbons each with six metal-jacketed waveguides.

6857-14

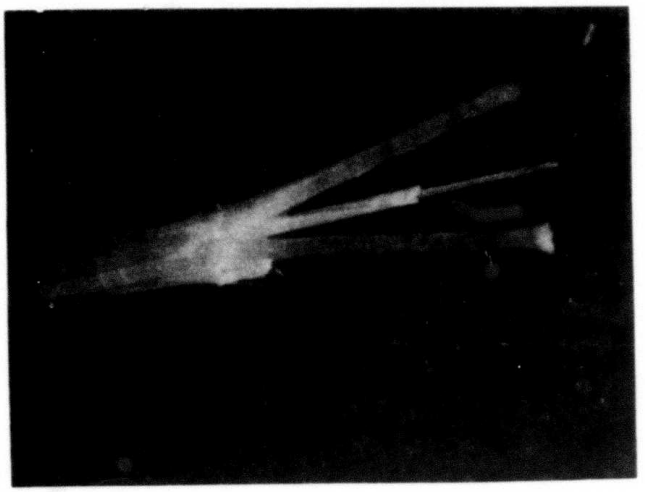

Figure 33.
Sample of ruggedized waveguide. The metal-jacketed waveguide (150 μm o.d.) is coated with a silastic buffer layer to reduce cabling-induced microbends and then surrounded by a fiberglass-resin composite. This structure will support a tensile load of 250 lb.

of work ahead requiring a well-planned technical effort. During this program we expect to address the major technical issues summarized below:

- Development of an extremely precise temperature control system for the metal coating tip. We have found that there is only a very narrow temperature range in which smooth continuous coatings of metal can be applied to the fiber. Above this range, pin holes and open areas develop in the metal coating. Below this range, the coating integrity is satisfactory, but the metal surface shows periodic ripples that contribute substantially to excess transmission loss caused by microbending.

- Expand our efforts, which have concentrated on aluminum coatings, to include more work with tin and tin alloy coatings. We have found that tin has a very fine dendritic crystalline structure and can form an exceedingly smooth outer surface when coated on the waveguide. This smoothness helps in minimizing microbending loss, and the fine structure will minimize the probability that a grain boundary imperfection will penetrate entirely through the metal jacket. There are several additional characteristics of tin that make it a good choice for our subsequent development. First, tin, unlike aluminum, is not chemically reactive in the presence of silica. Next, the oxide of tin can be more easily controlled and eliminated from the molten coating tip than can the very tenacious and durable oxide of aluminum. Finally, tin has a low recrystallization temperature, which permits spontaneous annealing of cyclically stressed fibers at and below ambient temperature.

- Develop procedures for making fiber waveguide preforms entirely by the modified chemical vapor deposition (CVD) technique. Currently, this technique is used only to make the preform cores while the cladding is formed from commercial silica tubing. We have found that the commercial grades of silica (including Suprasil) currently used to make waveguides contain many different types of flaws and inhomogeneities, which can lead to low strength sites in long glass fibers. Recognizing that the long-length strength of a fiber is determined by the weakest site, we have begun to catalog these flaws and have concluded that the only practical way to eliminate their influence is to form both the core and cladding of waveguide preforms by CVD. We plan to do this inside commercial tubing and then etch away the tubing, leaving a preform made entirely by CVD. Fiber waveguide

failures have sometimes been observed to originate from internal flaws. In all known cases, the initial flaw site was in the commercial silica cladding and not in the CVD core region. We believe this new preform fabrication procedure will not only eliminate occasional large flaws that result in low strength failures but may also allow us to produce fibers with minimum strengths approaching the 2,000,000 psi theoretical limit that has been calculated for fused silica. This limit is unachievable with plastic-coated fibers due to the static fatigue failure that would occur in less than 1 μsec. However, with hermetically protected fibers, it is reasonable to explore the possibility of realizing waveguides of exceptional strength. We have made a preliminary study of the economics associated with making all-CVD fibers and have concluded that this processing complication will increase cost only slightly.

- Fully characterize the optical transmission characteristics of waveguides under axial tensile loading. Results of initial measurements made at HRL indicate that transmission loss is a complex function of tensile stress in the fibers. Considerably more work on both metal- and plastic-coated fibers will be required to fully understand and control this effect.

- Establish proof-testing equipment and procedures that can be used to qualify the integrity of the metal coating and thereby assure the projected lifetime characteristics of the fibers. After reviewing the proof testing alternatives we had proposed to examine during our current effort, we have determined that one attractive method is to subject the fibers to a high proof test tensile load in the range of 650,000 psi using a modified version of the Hughes continuous tensile tester. This will be accomplished by extending the high tension section of the machine approximately 100 ft to a return pulley. The extension will be enclosed to contain a humid environment. During continuous proof testing, the fiber will dwell a sufficiently long time (several minutes) in the high tension section so that moisture attack through any pin holes and other imperfections in the metal coating would cause static fatigue failure with certainty. If the fiber does not fail this severe test, we can have high confidence in the integrity of the metal jacket.

  Another potentially useful technique is to utilize the light guiding properties of the waveguide to reveal the existence of any openings (defects) in the metal coating. We have already used this method off-line with completed metal-clad waveguides and are able to detect pinholes by

the escape of scattered light from the cladding region. We intend to investigate techniques for doing this type of inspection of the metal-clad waveguide in an on-line mode immediately after the metal sheath is applied.

- Determine the influence of the various dopants used in our silica waveguide structure on its static fatigue characteristics. Work to date has been limited to the verification that static fatigue can be eliminated in pure silica fibers by the use of hermetic metal jackets. It remains to be determined if common waveguide dopants, including B_2O_3, P_2O_5, and GeO_2, influence the static fatigue behavior. Work on composite glasses, including fiber glass, suggests that monovalent cation dopants, such as Na^{1+} in Na_2O, are sufficiently mobile that they can migrate to crack tips and accelerate failure and that divalent and higher valency cations are locked firmly into the host structure by their multiple bonds. On this basis, we expect B^{3+}, p^{5+}, and Ge^{4+} to be acceptable dopants. However, there is as yet no experimental data to confirm this tentative conclusion. We therefore plan to study the fatigue characteristics of various doped samples by the oblate bubble technique reported by Ernsberger.[1] Samples will be prepared at HRL by the CVD method using the semi-automated glass lathe normally employed for making fiber preforms. The samples will be tested by Professors J. Varner and J.D. McKenzie and their students in the Materials Science Division of the School of Engineering at UCLA.

[1] F.M. Ernsberger, Physics and Chemistry of Glasses, Vol. 10, p. 240-245 (December 1969).

SECTION 2

ACCOMPLISHMENTS

A. PROCESS CONTROLS

Considerable effort has been devoted in this period to examining the key process control parameters associated with the metal coating operation. A visual study of fracture surfaces resulting from low strength ($\leq$100 kpsi) ruptures during proof testing of Al-clad fibers revealed that a large fraction of these ruptures occurred at openings in the metal jacket. Figure 34 shows such a break that occurred in proof testing an Al-clad fiber. These openings have been frequently referred to as "pinholes" in the metal sheath. However, repeated microscopic photographs of these coating defects show that they are not pinholes but rather are large openings, typically having dimensions greater than the coating thickness. Figure 35(a) reveals the shape of a typical opening. The dimension perpendicular to the fiber axis is reasonably constant, whereas the length parallel to the fiber axis varies considerably from a minimum about like that in Figure 35(a) to very long openings running along the fiber for considerable distances, as shown in Figure 35(b). A key parameter in reducing the occurrence of these openings is the temperature of the metal coating tip. The openings can be eliminated entirely if the temperature is held within narrow limits. However, if it drifts out of the control range, even momentarily, then the probability of openings occurring increases rapidly. To avoid these chance departures from correct conditions, we have installed a special temperature control heating circuit using a proportional-type controller (Leeds and Northrop Electromax III). This control circuit, coupled with improved insulation to minimize thermal gradients caused by fluctuations in the environment, has been successful in achieving the necessary process control. Late in the quarter, we began fabricating long lengths (>500 m) of metal-clad fiber free of any visible openings. Some test results from one of these "defect free" fibers are discussed below.

Figure 34. Fiber break at an opening in the metal jacket. Recent proof test data reveal that a large fraction of the low strength ruptures are of this character.

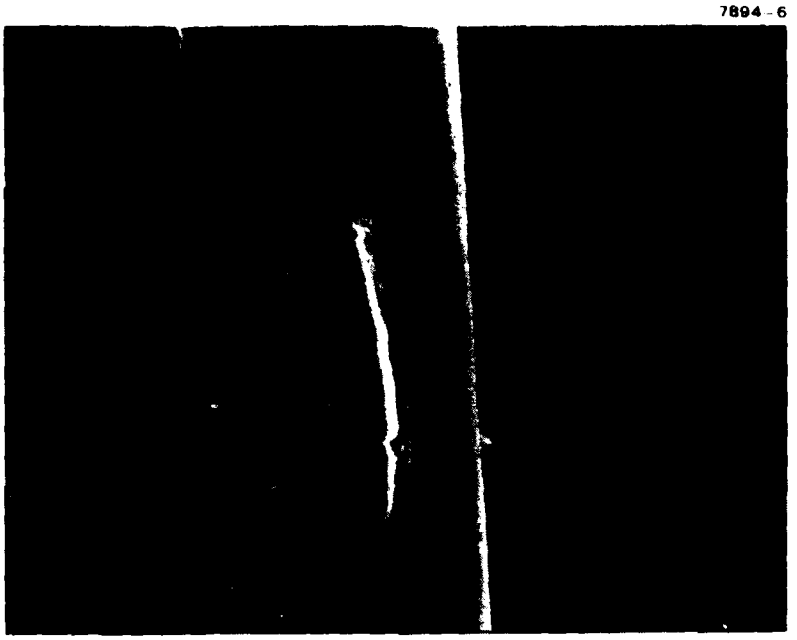

(a) Typical minimum-sized opening, approximately 50 μm wide and 200 μm long.

(b) Linear opening seen occasionally when coating parameters are not well controlled.

Figure 35. Typical opening defects in metal-jacketed fiber.

B. PROOF TESTING PROCEDURES

For quality assurance of metal clad fiber, it was recognized early that some method of inspection must be developed for detecting "pinholes" or openings that would leave the glass surface unprotected against mechanical abrasion and static fatigue. We have proposed that such openings could be detected by subjecting the fiber to humid conditions during proof testing for periods of time much longer than the static fatigue lifetime associated with the test stress level. To keep the test time to a practical level (say a few minutes per unit length of fiber), it is necessary to operate such a test at stresses near 600 kpsi, and in a test chamber at least 100 m long. Although such testing can be performed with an automatic proof tester that we have already developed, we would expect such testing to be inconvenient and expensive. Consequently, we have been searching for alternate approaches to verifying the mechanical integrity of metal-clad fiber. During our studies of openings in the metal coating (as discussed above), we have observed that there appears to be a minimum size to this type of coating flaw and also that there is ample light scattered out through this minimum opening for ready detection. Thus, we are now developing a "candling" technique for examining the fiber immediately after the metal coating is applied. By continued examination of low strength ruptures and the collection of more statistics on the size of openings, we should be able to verify the usefulness of the candling method. This type of test can be conducted off-line for metal-clad waveguide by using an He-Ne laser as the light source and observing the radiation scattered out through any openings. There is sufficient Rayleigh scattering at the He-Ne wavelength in the waveguide core to keep detectable quantities of energy in the cladding (or nonguiding) modes along at least a 1-km length of waveguide. For metal-coated quartz fibers without waveguiding cores, such as are used for process control and strength studies, the candling must be done in the region immediately after the coating tip. In that region, there is still sufficient light guided down the fiber from the high-temperature drawing region ($T > 2000°C$) to be readily detectable. Because such fibers do not guide light except for short distances because of strong absorption

of the evanescent field by the metal cladding, off-line candling is not practical for lengths beyond a fraction of a meter.

C. OTHER METALS

During the first quarter, some preliminary coating with metals other than aluminum was attempted. Because of the problems of temperature control mentioned above, none of this work led to improved high-strength fibers. In short test sections (0.5 m), a few high-strength specimens (>500 kpsi) were obtained with coatings of both Zn and an Al-Si alloy. However, the presence of openings in both of these coatings was pronounced and resulted in many low-strength breaks. Further work with Sn cladding confirmed the good strengths (up to 900 kpsi) obtained earlier but also revealed the susceptibility of the Sn jacket to mechanical disruption which leads to low strength ruptures. Preliminary attempts during this quarter to provide a protective plastic overcoat for the Sn-clad fiber have been unsuccessful. However, because of the high strengths already observed, further work to protect the tin cladding is justified, and we will be pursuing several approaches during this program.

D. OPTICAL CHARACTERIZATION

During much of this quarter, the facilities for measuring spectral insertion loss were being modified (under complementary IR&D support) to allow semi-automatic measurements. To the apparatus already shown in Figure 17, a stepping motor for driving the spectral scan has been added and the output of the lock-in amplifier is now fed directly through a microprocessor to a dedicated HP 9825 computer, which processes the data, stores them, and controls the spectral scan. After data have been collected on both long and short samples, the computer compares the two sets of data, computes the spectral attenuation, and outputs it to an X-Y plotter. With this new system, the time required to obtain a spectrally scanned measure of waveguide attenuation has been reduced several fold. This same technique is also being extended to the optical time domain reflectometer (see Figure 18) for both loss and pulse-dispersion measurements.

As discussed earlier, a preliminary evaluation of the effect of tensile loads on the optical attenuation in fiber waveguides gave some interesting but inconclusive results. We have now located an isolated tunnel where sections of waveguide longer than 200 m can be deployed and subjected to axial tensile loading. Apparatus is now being assembled to measure the spatially resolved attenuation along the fiber length by OTDR techniques. The length of fiber under test is sufficient to permit attenuation to be determined in the center section of the specimen without interference from any termination effects that might be present. We expect these measurements to be started, but probably not completed, by the end of the next quarter.

E. FATIGUE STUDIES IN DOPED SILICA

The purpose of this task is to determine the feasibility of using the so-called oblate bubble technique to measure the extent of static fatigue in doped fused silica used in optical waveguides. This investigation is being carried out under a research subcontract to the Materials Department at UCLA. Drs. J.D. Mackenzie and J.R. Varner are the principal investigators. During the first quarter, the following tasks were identified and initiated:

- Making suitable specimens
- Developing tensile test procedures
- Achieving fracture initiation at the bubble surface.

The high softening point and high viscosity of fused silica make specimen preparation difficult, but the glass working shop at UCLA has succeeded in producing suitable specimens from TO-8 Amersil capillaries. After forming the oblate bubble in each specimen, a central region, about 12 mm long, is ground to a diameter of about 4 mm (the diameter of the original rod is about 6.25 mm). The specimen is then etched in an HF solution, fire polished, and then coated with a thin layer of Sylgard 182 silicone rubber.

Bubble geometry is determined by immersing specimens in Nujol ($n \cong 1.5$) and measuring the major and minor axes. From these measurements, the radius of curvature can be calculated. This work is done prior to HF etching and fire polishing. To date, most bubbles have had major axes < 1 mm and minor axes < 0.2 mm.

Partial success has been achieved in developing a tensile test procedure. A brass ferrule is attached to each end of a specimen using rapid-setting cyanoacrylate adhesive. A tight fit between ferrule and rod is important to achieve correct alignment of the specimen. Because of variations in the rod diameters, it is necessary to have a selection of ferrules with a range of inner diameters. The ferrules fit into nuts which are screwed onto threaded metal connectors which in turn are attached to the load cell and crosshead, respectively, using universal joints. Using this procedure, about 35% of the breaks have originated at the central necked-down portion of the specimens. Further refinement of the procedure is needed to raise this percentage.

To this point, no breaks have originated at the bubble surfaces. There are two possible explanations:

- The bubbles have been relatively small (major axis < 1 mm). The glass blower has been asked to make the bubbles larger ($\sim$1.5 x 0.15 mm). This would give a radius of curvature of $\sim$0.0075 mm and a stress concentration factor of about 13.5.

- Grinding the central section causes severe subsurface damage. Longer etching times will be used in the hopes of eliminating this damage prior to fire polishing.

F. TREATMENT OF FIBER STRENGTH DATA

The stochastic nature of the size distribution of surface flaws which control the breaking strength of brittle materials like silica requires a probabilistic approach in describing the strength of the material. Therefore, it is customary to characterize the tensile strength of silica fibers by a distribution function relating the probability of survival (or failure) to the applied stress. For this purpose, the

Weibull distribution[1] has found wide use. It is relatively easy to calculate and, for test specimens of a particular length, it explicitly shows the cumulative probability of failure as a function of applied stress. This probability is obtained directly from the test results by the methods of order statistics in which the weakest sample is assigned the lowest probability of failure (equivalent to the reciprocal of the number of samples). The next strongest sample corresponds to a cumulative failure probability of twice the reciprocal of the number of samples and so on for each successively stronger test specimen. From this there results a diagram of the type already seen in Figure 10. Because the probability of failure (or survival) is a length-dependent parameter, data from test samples of varying gauge lengths must be properly adjusted if they are to be displayed on a single Weibull plot. The methods for doing this are straightforward.

If one wishes to add proof test data to data from fixed-gauge-length specimens, then it is necessary to calculate a new statistic since the ruptures in the proof test are not "ordered" (or ranked by strength). The most convenient statistic to use is the number of breaks at a particular stress level that occur per unit length of specimen. From this statistic, the probability of failure for the gauge length of interest can be calculated, thus permitting the proof test results to be put onto a Weibull plot corresponding to that same gauge length. This procedure has been followed by many workers and is described for example by Kalish et al.[2]

---

[1] W. Weibull, "A Statistical Distribution Function of Wide Applicability," J. Appl. Mech. 18, 293-297 (1951).

[2] D. Kalish, B.K. Tariyal, and R.O. Pickwick, "Strength Distributions and Gage Length Extrapolations in Optical Fibers," Ceramic Bull. 56, 491-503 (1977).

Last year, Helfand and Wasserman[1] of Bell Laboratories reviewed the statistical treatment of strength data for optical fibers. One of their recommendations was to employ a statistic known as the "cumulative hazard" for characterizing the distribution of breaking strengths. We followed their suggestion and have come to the conclusion that the cumulative hazard statistic offers several advantages that make it more useful to the fiber technologist than the conventional Weibull treatment. In treating strength data, both from our own tests and from the work of others, we have found the key features to be:

- In common with the Weibull method, the hazard statistic is based on "order statistics" and is readily calculated with desk top computers. It also leads to linear regions of data and readily indicates where changes in failure mechanisms and/or flow distributions occur. Calculations of probability of survival or failure are easily made for any length of fiber over the stress range covered by the test data.

- The cumulative hazard function represents the average density of flaws larger than a specified size per unit length of fiber and hence denotes a physical characteristic that is of prime concern to the technologist.

- Data obtained on tensile test specimens of various lengths can be combined in a single graph without the need for any assumptions about linearity or constancy of failure modes.

- Perhaps the most practical characteristic is that quantitative proof test data can be directly plotted on the same graph as normal tensile test data. This greatly facilitates the study of the "weak tail" of the strength distribution.

For many years, the hazard function has been used in the analysis of lifetime data for objects each having a failure rate that is a function of its age.[2] This function is also known as the "intensity function" or the

---

[1] E. Helfand and Z.R. Wasserman, "Statistics of the Strength of Optical Fibers," JAP 48, 3251-3259 (1977).

[2] K.V. Bury, "Statistical Models in Applied Science," John Wiley & Sons, NY, 1975, p. 327ff

"force of mortality." Nelson[1] discussed the application of this method to breaking strength data and thus set the stage for the later use of these methods by Helfand and Wasserman.[2] Refs. 2, 3, and 4 discuss the derivation of the key relationships of extreme value statistics. We will confine our discussion here to those equations necessary to apply the method to optical fiber strength distributions and to the relevant assumptions involved. This treatment follows that of Ref. 2. As in the treatment of failure in all brittle materials, the key assumptions are that (1) the "weakest-link theory" is applicable (i.e., a fiber will break when the stress exceeds the strength of the weakest section along its length, and (2) the probability distribution of each point is independent of the strength at other points. Under these reasonable assumptions, the cumulative probability that a fiber of length L will fail at or below a stress s can be written in the form

$$P_f(s,L) = 1 - \exp\,[-\,L \cdot H(s)]\ , \qquad (1)$$

where H(s) is the "cumulative hazard," here expressed on a per unit length basis. Because H(s) is independent of L, it makes a more useful parameter for studying strength data than does $P_f(s,L)$, which contains a length dependence.

---

[1] W. Nelson, "Theory and Applications of Hazard Plotting for Censored Failure Data," Technometrics 14, 945-966 (1972).

[2] E. Helfand and Z.R. Wasserman, "Statistics of the Strength of Optical Fibers," JAP 48, 3251-3259 (1977).

[3] K.V. Bury, "Statistical Models in Applied Science," John Wiley & Sons, NY, 1975, p. 327ff.

[4] E.J. Gumbel, "Statistics of Extremes," Columbia University Press, NY, 1958.

The cumulative hazard H(s) has a simple physical interpretation that makes it very useful in the case of uncorrelated flaws. Consider a flaw C_s that, when present in a fiber or on its surface, will cause a break at a stress $\leq s$. Then H(s) is defined as the lineal density of C_s flaws on the fiber (i.e., the number of C_s flaws per unit length of fiber). Equivalently, 1/H(s) is the average spacing between C_s flaws.

To display data obtained from fixed gauge length tests and thus reveal the flaw density distribution as a function of the stress s, one needs to calculate H(s). This is accomplished in a manner quite similar to the data treatment employed in Weibull plotting. The samples are ordered by their strength and assigned an index number k, where k = 1 is assigned to the weakest sample, k = 2 to the next weakest sample, and so on up to k = n for a test population of n samples. Thus, $s_1 \leq s_2 \leq \ldots s_k \leq \ldots \leq s_n$. It is not necessary that all of the samples have the same length although the arithmetic is much simpler if they do. For purposes of explanation, we shall assume that each sample has a constant length ΔL and that the total length L of sample in the test population is therefore $L = n\,\Delta L$. The extension of the calculation of H(s) to cases where ΔL is not a constant is straightforward.

For the sample breaking at s_1, the lowest strength, there was only one flaw of the size C_s in the entire length of fiber L. Hence, the measured lineal density of this flaw is just 1/L. This quantity we call $H(s_1)$. For the second strongest piece, which broke at s_2, the measured concentration of flaw sizes capable of causing breaks at stresses in the interval $s_1 < s \leq s_2$ is one flaw in the sample length $(L - \Delta L)$, where we have removed from consideration the length of sample which broke at s_1. Therefore, the measured concentration of flaws capable of causing breaks at any stress $\leq s_2$ is just the sum of the concentration $1/L + 1/(L - \Delta L)$. This quantity is by definition $H(s_2)$. By extension to samples of increasing strength, we obtain a general formula for calculating the cumulative hazard in terms of the length L_m of sample remaining before the m-th break:

$$H(s_k) = \sum_{m=1}^{k} \frac{1}{L_m} \quad .$$

For samples of uniform length ΔL, the quantity L_m is given by the expression $L - (m - 1)\,\Delta L$. For a given value of ΔL and a population of n samples, the values of $H(s_k)$ for k = 1 to n can be calculated on a desk top computer by simple recursion formulas. (If ΔL is not a constant, then this calculation must be performed step-wise with insertion of each $\Delta L(k)$ so that the proper value of L_m is obtained for each k.) Ref. 1 gives a more rigorous discussion of the cumulative hazard statistic and its estimation from experimental data.

A plot of log $H(s_k)$ versus log s_k produces a graph which looks very similar to a Weibull plot. Because much of the breaking strength data follows a power law distribution, both the Weibull and the cumulative hazard plots show linear regions from which empirical constants such as the slope and intercept can be calculated. In the Weibull method, these parameters are needed for calculations of failure probability for fiber lengths different from those which were tested. On a cumulative hazard plot, such extrapolations can be made graphically and the risks involved in this extrapolation seem to us to be much more obvious to the technologist. For example, a cumulative hazard plot containing proof test results readily indicates the onset of the "low end tail" in the strength distribution. With such data, one quickly recognizes the danger in predicting the strengths of long lengths of fiber from the often very impressive data taken on short specimens.

The inclusion of proof test data into a cumulative hazard plot is quite straightforward. The concentration of flaws causing breaks at s_1, the lowest proof test level, can be obtained by dividing the total number of breaks by the total length of fiber tested. For the next level, s_2, the calculation is repeated and the result is added to the result for s_1 to get the cumulative flaw concentration, $H(s_2)$, leading to breaks at $s \leq s_2$. No extrapolations are required to plot data from one sample length to another. In Figure 36, we have plotted typical data obtained during the past year for Al- and Sn-clad Suprasil 2 fibers. For convenience, we have plotted only enough data points to show the general shape of the strength

[1] E. Helfand and Z.R. Wasserman, "Statistics of the Strength of Optical Fibers," JAP 48, 3251-3259 (1977).

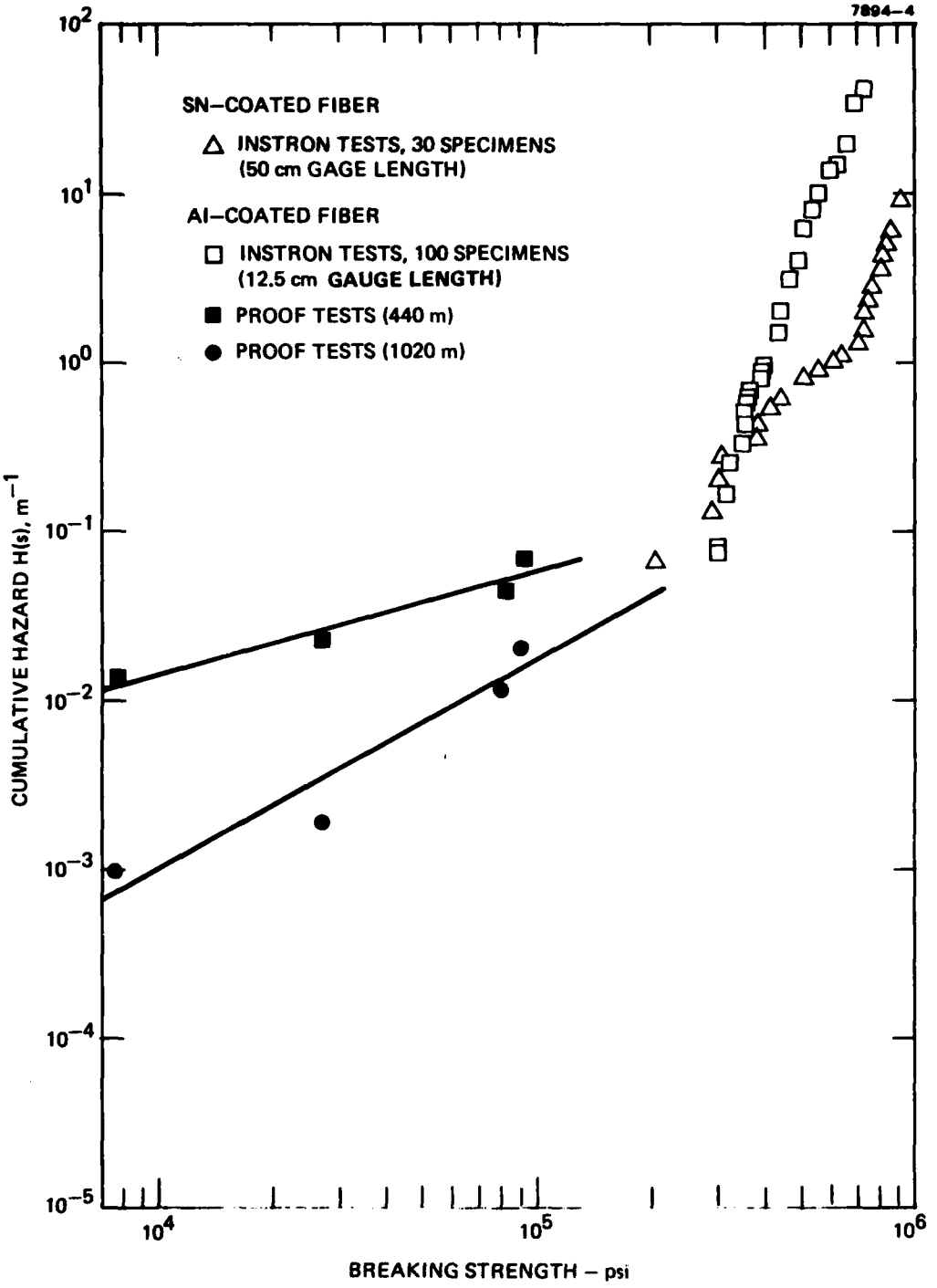

Figure 36. Strength distributions for early Al- and Sn-clad fibers. The proof test data from long lengths of fiber clearly reveal the existence of a "low end tail," or occasional large flaws.

distribution. For Al-clad fibers, the flaw distribution changes dramatically near a stress level of about 300 kpsi. Failure at this stress is attributed by the Griffith theory to a flaw depth of about 250 Å, and as the figure shows, flaws of this magnitude are occurring, on the average, about once in every 10 m of fiber for coatings of both Sn and Al. As yet we have been unable to conduct proof tests on Sn-clad fibers. The soft Sn jacket is not tough enough to withstand the rigors of the proof test procedures associated with the dynamic loading encountered in the laboratory proof tester (see Figure 13). Later in this program, we will investigate the use of plastic overcoats as a means of protecting the Sn coating from serious disruption during tests and subsequent deployment.

One task in the present program is to identify and eliminate the causes of the infrequent large flaws revealed in Figure 36. As mentioned above, we now believe that openings in the metal coating are a likely source of surface damage, particularly during proof testing, and are probably a major contributor to the low strength characteristics. As this quarter ended, we had started to draw metal-coated fiber substantially free of openings and will have some test results soon.

G. ALL SYNTHETIC GLASS PREFORMS

At the request of the COTR, work on this task has been rescheduled to start in the third quarter of the program.

H. CABLING STUDIES

Work on this task will be initiated next quarter with the investigation of commercially available protective plastic overcoats.

I. COMPLEMENTARY ACTIVITIES

As part of our overall IR&D effort in high strength fiber technology, a new fiber drawing facility is being developed. The structure for the drawing tower has been designed and construction will begin next quarter. The drawing furnace has been ordered and is scheduled for delivery late

in the next quarter. We expect to have a newly prepared drawing room, containing two drawing assemblies and necessary supporting equipment, in operation by about the end of the third quarter (January 1979).

In selecting the heat source for the new drawing facility, we have been influenced by recent good results on very long lengths of high-strength plastic-coated fiber prepared at Bell Laboratories in an induction-heated furnace using air-stable ZrO_2 muffle tubes. The induction furnace has the advantage of rapid warm-up and cool-down as well as very long life for the furnace components. The ZrO_2 muffle tubes are especially stable in air and, when properly treated, have yielded fiber of exceptionally good strength in long lengths. Work with this type of heat source has been going on for several years at Bell Laboratories, and some results were recently reported by DiMarcello.[1] To illustrate their impressive results, we have plotted DiMarcello's proof test data on a cumulative hazard plot (as discussed in the previous section) in Figure 37. These results were obtained on a total test length of 10 km and, to our knowledge, represent the best results yet published.

DiMarcello's data can be used to quickly calculate the likelihood of fibers of this quality surviving the application of any given stress level for a period of time short compared to the static fatigue lifetime at that stress level. As we have already seen, the cumulative probability of failure, $P_f(s,L)$, of a fiber of length L at any stress level $\leq s$ is given by the expression

$$P_f(s,L) = 1 - \exp\,[-H(s) \cdot L] \quad ,$$

where H(s) is the cumulative hazard expressed in units of reciprocal length. By definition, the probability of survival, $P_s(s,L)$, under these conditions is just

$$P_s(s,L) = 1 - P_f(s,L) \quad .$$

---

[1] F.V. MiMarcello, A.C. Hart, Jr., J.W. Williams, and C.R. Kurkjian, "High Strength Furnace Drawn Optical Fibers," Conference on Physics of Fiber Optics, Kingston, RI, 22-23 June 1978.

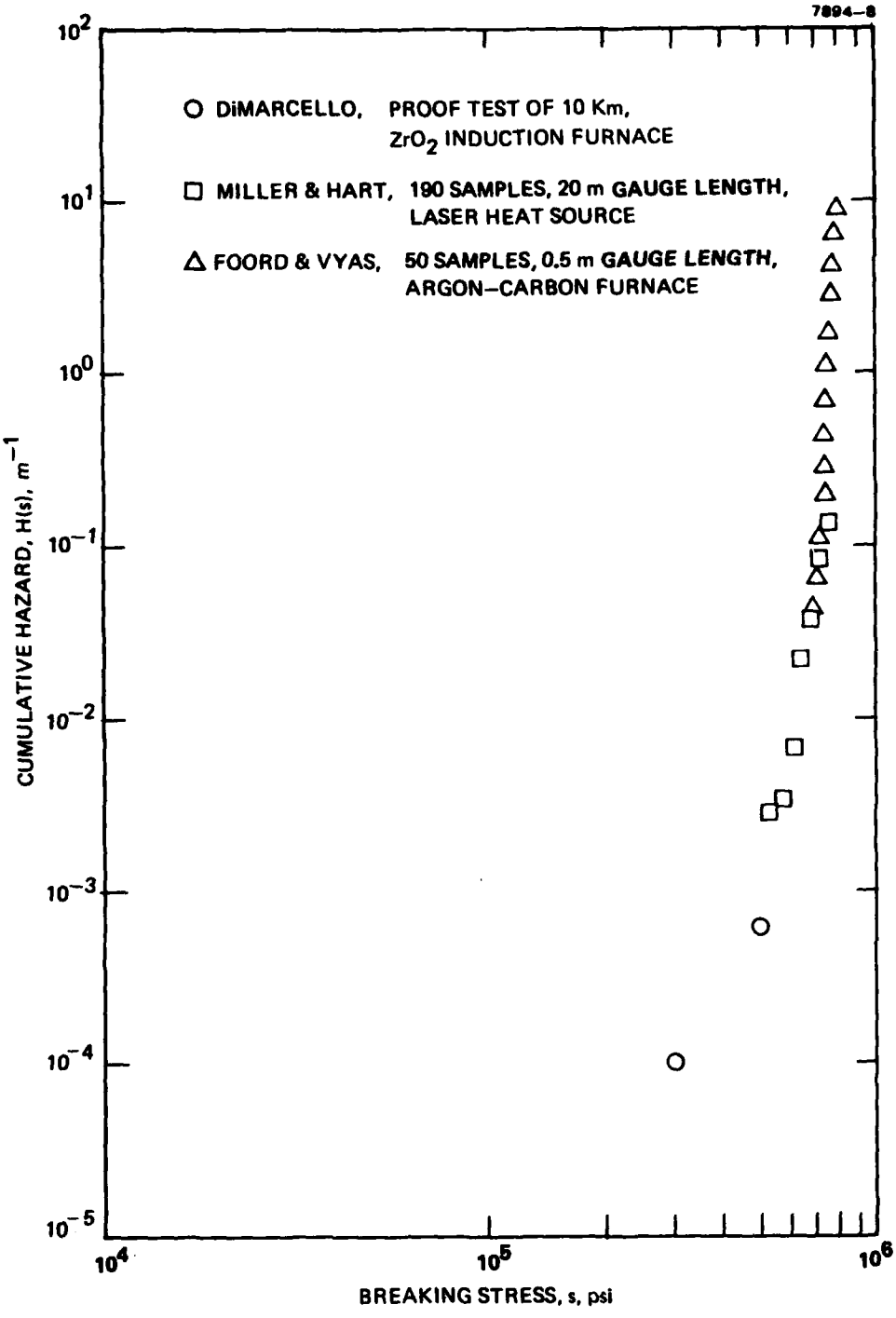

Figure 37. Strength distributions for plastic-clad fibers drawn with different heat sources. The results of DiMarcello obtained with the ZrO_2 induction furnace are the most impressive long-length data yet published.

Thus, we see that

$$P_s(s,L) = \exp [-H(s) \cdot L] \quad .$$

Applying this relationship to DiMarcello's proof test results indicates that 90% of all 1-km lengths should survive a short time stress level of 300 kpsi. If we extrapolate the experimental results to 200 kpsi, we would expect 78% of all 10-km lengths to survive a 200 kpsi load. These are very encouraging projections.

Prior to this time, the best long-length high-strength fiber has been obtained by the use of a laser heat source. The recent data of Miller and Hart[1] with laser-drawn fiber are also plotted in Figure 37 for a 3.4-km-long sample. Good results from a carbon resistance furnace with an argon-atmosphere-protected carbon muffle tube have also been obtained for short sections of fiber.[2] These data are also plotted in Figure 37.

These results appear consistent with those of DiMarcello and suggest that the troublesome low-strength breaks can be eliminated with proper attention to drawing conditions for a variety of heat sources. We believe that the induction furnace approach has good potential for trouble-free economic operation. It can be used equally well with either oxidizing conditions (ZrO_2 muffle in air or O_2) or neutral (or slightly reducing) conditions employing a carbon muffle tube protected by argon or other oxygen-free gas environments. With our new drawing facility, we expect to make rapid progress toward substantially reducing or eliminating the "low end tail" (as seen in Figure 36 for our earlier metal-clad fibers).

---

[1] T.J. Miller and A.C. Hart, "Effects of Preform Surface Treatment on the Tensile Strength of Silicone Coated Silica Fibers," to be published.

[2] S.G. Foord and M.K.R. Vyas, "Tensile Strength Measurements on Plastic-Coated Optical Fibers," Colloquium on Optical Fibre Cable, Professional Groups E13 and S^2, IEE, London, 17 May 1977.

SECTION 3

PLANS FOR THE NEXT QUARTER

Work will continue on all tasks discussed in Section 2. Specifically, we expect to have reportable results in the following areas:

- Effect of coating process control on elimination of open defects in the metal cladding.
- Improvement in long-length strength distribution resulting from elimination of open defects.
- Establishment of, and perhaps some early results from, test facility for measuring excess optical attenuation caused by axial strain.
- Finalization of sample preparation and handling techniques for the oblate bubble static fatigue studies.
- Initiation of protective plastic overcoat studies for both ruggedization and corrosion protection.